J Neurophysiol 114: 2353–2367, 2015.
First published August 19, 2015; doi:10.1152/jn.00926.2014.

Open-loop organization of thalamic reticular nucleus and dorsal thalamus: a computational model

Adam M. Willis,[1,2] Bernard J. Slater,[3] Ekaterina D. Gribkova,[4] and Daniel A. Llano[3,4,5]

[1]*Department of Neurology, San Antonio Military Medical Center, Fort Sam Houston, Texas;* [2]*Department of Theoretical and Applied Mechanics, University of Illinois at Urbana-Champaign, Urbana, Illinois;* [3]*Neuroscience Program, University of Illinois at Urbana-Champaign, Urbana, Illinois;* [4]*Department of Molecular and Integrative Physiology, University of Illinois at Urbana-Champaign, Urbana, Illinois; and* [5]*Beckman Institute for Advanced Science and Technology, Urbana, Illinois*

Submitted 18 November 2014; accepted in final form 17 August 2015

Willis AM, Slater BJ, Gribkova ED, Llano DA. Open-loop organization of thalamic reticular nucleus and dorsal thalamus: a computational model. *J Neurophysiol* 114: 2353–2367, 2015. First published August 19, 2015; doi:10.1152/jn.00926.2014.—The thalamic reticular nucleus (TRN) is a shell of GABAergic neurons that surrounds the dorsal thalamus. Previous work has shown that TRN neurons send GABAergic projections to thalamocortical (TC) cells to form reciprocal, closed-loop circuits. This has led to the hypothesis that the TRN is responsible for oscillatory phenomena, such as sleep spindles and absence seizures. However, there is emerging evidence that open-loop circuits are also found between TRN and TC cells. The implications of open-loop configurations are not yet known, particularly when they include time-dependent nonlinearities in TC cells such as low-threshold bursting. We hypothesized that low-threshold bursting in an open-loop circuit could be a mechanism by which the TRN could paradoxically enhance TC activation, and that enhancement would depend on the relative timing of TRN vs. TC cell stimulation. To test this, we modeled small circuits containing TC neurons, TRN neurons, and layer 4 thalamorecipient cells in both open- and closed-loop configurations. We found that open-loop TRN stimulation, rather than universally depressing TC activation, increased cortical output across a broad parameter space, modified the filter properties of TC neurons, and altered the mutual information between input and output in a frequency-dependent and T-type calcium channel-dependent manner. Therefore, an open-loop model of TRN-TC interactions, rather than suppressing transmission through the thalamus, creates a tunable filter whose properties may be modified by outside influences onto the TRN. These simulations make experimentally testable predictions about the potential role for the TRN for flexible enhancement of cortical activation.

burst; T-type calcium channels; thalamic reticular nucleus; thalamocortical neurons; thalamus

THE THALAMUS is a critical checkpoint for all information that reaches the cerebral cortex. Despite many decades of scientific investigation, its role in sensory information processing has remained unclear. One key to understanding the role of the thalamus likely lies in its interactions with a closely related and mysterious structure known as the thalamic reticular nucleus (TRN). The TRN is a thin layer of GABAergic neurons that partially surrounds the dorsal thalamus,[1] and its neurons innervate thalamocortical (TC) neurons (Pinault 2004). The TRN has been widely speculated to play prominent roles in a host of brain functions, such as maintenance of arousal (Llinás and Paré 1991; Steriade et al. 1993a), selective attention (Crick 1984; Guillery et al. 1998; McAlonan et al. 2008), the production of sleep spindles (Destexhe et al. 1994), and, in pathological states, the production of seizures (McCormick and Contreras 2001), and may contain functional subnetworks subserving these myriad functions (Halassa et al. 2014). Despite the wealth of data derived from slice physiological studies about the TRN, the specific role of the TRN in modulating larger-scale brain activity has been difficult to elucidate, in part because the TRN is a small, deep structure and therefore difficult to study in vivo. For this reason, computational models can be used to build bridges between the microcircuit-level analysis of the TRN and network-level phenomena.

TRN neurons receive input from branches of TC axons en route to the cortex as well as branches from corticothalamic axons en route to the thalamus (Pinault 2004). Early models of TRN function postulated that TC neurons and TRN neurons are reciprocally innervated (Steriade et al. 1993a). Models including reciprocal thalamic-TRN innervation reproduce well-known oscillatory phenomena thought to be generated in the thalamus, such as spindle oscillations and absence seizures (Destexhe et al. 1993, 1999; Huguenard 1998). However, there are emerging data suggesting that there are additional nonreciprocal or open-loop arrangements between the thalamus and TRN. For example, the TRN receives input from regions of the thalamus that do not receive returning axons from the TRN (Crabtree and Isaac 2002; Kimura 2014; Kimura et al. 2007; Pinault and Deschênes 1998). In addition, the sensory portions of the TRN receive input from nonsensory parts of the forebrain, such as the prefrontal cortex (Zikopoulos and Barbas 2006), basal forebrain (Asanuma and Porter 1990; Bickford et al. 1994; Pita-Almenar et al. 2014; Sun et al. 2013), and amygdala (Zikopoulos and Barbas 2012). These types of open-loop circuits may provide a substrate by which TC transmission may be modulated by regions of the brain not classically associated with sensory processing, possibly to permit attentional or emotional demands to modify sensory processing.

A key component for the potential of the TRN to shape the coding properties of the thalamus is the low-threshold bursting behavior of TC neurons. Hyperpolarization of TC neurons leads to deinactivation of T-type calcium channels, which changes the response mode of TC cells from tonic, single-spike firing to low-threshold, burst firing (Jones 2007; Sherman 2001). Low-threshold bursting allows hyperpolarized thalamic neurons not only to respond to stimuli that would normally be

Address for reprint requests and other correspondence: D. A. Llano, 2355 Beckman Inst., 405 N. Mathews, Urbana, IL 61801 (e-mail: d-llano@illinois.edu).

[1] Note that many authors use the term "dorsal thalamus" to refer to the structure that is commonly called "thalamus." In this report, for simplicity, the word "thalamus" does not refer to ventral thalamic structures such as the TRN.

subthreshold but also to respond to such stimuli with a burst of two to five action potentials. Previous experimental and computational work has established that bursts are a reliable way to send a high-efficacy signal to a postsynaptic target and are likely a more suitable mode for signal detection than spikes in tonic mode (Denning and Reinagel 2005; Goense et al. 2003; Krahe and Gabbiani 2004; Lisman 1997; Mukherjee and Kaplan 1995; Person and Perkel 2005; Reinagel et al. 1999; Smith et al. 2000; Swadlow and Gusev 2001). In the case of the TC synapse, since this synapse induces large postsynaptic currents but is highly depressing (Chung et al. 2002; Gil et al. 1999; Stratford et al. 1996), a burst of action potentials arriving after a period of quiescence (as required by the voltage- and time sensitivity of T-type calcium channels) would have a high likelihood of inducing a postsynaptic response in a cortical neuron. In contrast, thalamic cells in "tonic" mode have a lower likelihood of inducing a cortical response because the tonically arriving individual spikes would likely meet a depressed synapse. Therefore, the TRN appears poised to induce a switch from tonic to burst firing based on its ability to hyperpolarize TC neurons. However, because of the time required to deinactivate the T-type calcium channels (Jahnsen and Llinas 1984), the TRN may also simply suppress incoming signals to the thalamus if those signals arrive prior to T-channel deinactivation. Therefore, the TRN is strategically situated to influence the flow of information passing through the thalamus and may enhance or suppress thalamic responsiveness, depending on the relative timing of afferent inputs and TRN activation.

An important consideration for any theory of thalamic function that involves the use of bursts as a means to carry sensory information is whether or not bursts are seen during the awake state. Several studies have shown that a mixture of bursting and individual spikes is seen in awake animals (Fanselow et al. 2001; Guido and Weyand 1995; Ortuño et al. 2014; Ramcharan et al. 2005), suggesting that the excitability of thalamic neurons may be actively modulated during wakefulness. This is consistent with the finding that injection of currents into thalamic cells in vitro, similar to those recorded in vivo, produces a mixture of single spikes and bursts (Wolfart et al. 2005). It is also important to note that bursts per se are not critical for the potential for the TRN to boost thalamic output. This is because the low-threshold potentiation of depolarization created by T currents, which may only produce one or two spikes riding a slow calcium wave, may also enhance cortical activation. Because these spikes necessarily follow a period of quiescence, they would not be subject to the strong temporal filtering at the TC synapse (Deleuze et al. 2012).

Therefore, given *1*) the presence of extrinsic inputs from remote brain regions onto TRN neurons, *2*) the potential for TRN neurons to potentiate thalamic output by creating bursts, and *3*) the strong temporal filtering present at the TC synapse, we hypothesized that stimulation of the TRN could paradoxically enhance cortical responses to sensory stimuli. Furthermore, we hypothesized that this enhancement would only be seen at particular rates of TRN and sensory input. To test these ideas and to generate quantitative predictions that could be tested experimentally, we constructed a computational model containing TC cells, TRN cells, fast-spiking (FS) interneurons, and thalamorecipient cells in layer 4 (L4) of the cortex and explored the dynamics of this network as TRN inputs were modulated. Preliminary results of this work were previously presented in abstract form (Willis and Llano 2012).

METHODS

All surgical procedures were approved by the Institutional Animal Care and Use Committee at the University of Illinois. All animals were housed in animal care facilities approved by the Association for Assessment and Accreditation of Laboratory Animal Care International. Every attempt was made to minimize the number of animals used and to reduce suffering at all stages of the study.

Physiological recordings. Balb/c mice (30–40 days of age) were bred in house from breeders purchased from Harlan Laboratories. To obtain slices, mice were deeply anesthetized by intraperitoneal injection of pentobarbital (50 mg/kg), then transcardially perfused with an ice-cold high-sucrose cutting solution (in mM: 206 sucrose, 10.0 $MgCl_2$, 11.0 glucose, 1.25 NaH_2PO_4, 26 $NaHCO_3$, 0.5 $CaCl_2$, 2.5 KCl, pH 7.4), and had brains removed quickly. Coronal tissue slices (300 μm) were cut with a vibrating tissue slicer and transferred to a holding chamber containing oxygenated incubation artificial cerebrospinal fluid (aCSF; in mM: 126 NaCl, 3.0 $MgCl_2$, 10.0 glucose, 1.25 NaH_2PO_4, 26 $NaHCO_3$, 1.0 $CaCl_2$, 2.5 KCl, pH 7.4) and incubated at 32°C for 1 h prior to recording.

Whole cell recordings were performed with a visualized slice setup outfitted with infrared-differential interference contrast optics and performed at 32°C. During recordings, tissue was bathed in recording aCSF (in mM: 126 NaCl, 2.0 $MgCl_2$, 10.0 glucose, 1.25 NaH_2PO_4, 26 $NaHCO_3$, 2.0 $CaCl_2$, 2.5 KCl, pH 7.4). Recordings were done in the absence, and the presence, of tetrodotoxin (TTX). TTX was added to the bath at a 1 μM concentration to eliminate spikes to permit parameter matching for the underlying membrane properties (see below). Recording pipettes were pulled from borosilicate glass capillary tubes and had tip resistances of ~5 MΩ when filled with solution, which contained (in mM) 117 K-gluconate, 13 KCl, 1.0 $MgCl_2$, 0.07 $CaCl_2$, 0.1 ethylene glycol-bis(β-aminoethyl ether)-*N, N, N′, N′*-tetraacetic acid, 10.0 4-(2-hydroxyethyl)-1-piperazineethanesulfonic acid, 2.0 Na-ATP, 0.4 Na-GTP, and 0.5% biocytin, pH 7.3. Thalamic areas were identified via landmarks readily visualized in the slice. The data for the present study come from neurons in the ventral posterior medial part of the thalamus, from the TRN, and from FS and regular-spiking cells in cortical L4. We used the Multiclamp 700B amplifier (Molecular Devices, Sunnyvale, CA) and pCLAMP software (Molecular Devices) for data acquisition (20-kHz sampling). Multiple cells were recorded from each class (TC, TRN, L4 regular spiking and FS). A representative neuron from each class was chosen to be modeled. This approach was used rather than averaging parameters across neurons because using parameter averages may lead to modeling of cell parameter combinations that may not exist in reality. Our choice of modeling representative neurons still allows exploration of a broad range of parameters to examine the impact of those parameter changes on model performance (e.g., Fig. 8).

Model architecture. Single-compartment models of TC, TRN, FS, and L4 cells were built with a Hodgkin-Huxley framework with membrane potential V modeled by the first-order differential equation for a single-compartment neuron:

$$C_m = \frac{dV}{dt} = g_L(V - E_L) + \sum_{i=1}^{n} g_i(V)(V - E_i) + I_e$$

where g_L is the leak conductance, E_L is the leak reversal potential, C_m is the capacitance of the membrane, n is the number of channels, $g_i(V)$ is the conductance of the ith channel, E_i is the reversal potential of the ith channel, and I_e is the externally applied current to the cell. The conductances of each channel are semiempirically modeled by activation and inactivation variables. Our TC model used the same model as Deleuze et al. (2012) and included a T-type calcium channel, an H current, as well as fast sodium current and delayed rectifying potas-

sium current. For complete mathematical description of model, please refer to Deleuze et al. (2012). A similar computational model was also used to describe the dynamics of TRN cells, with parameters changed to match physiological recordings from TRN cells. A slow-inactivating potassium current (KS current; Pospischil et al. 2008; Yamada et al. 1989) was added to this model to account for spike-frequency adaptation seen in our TRN recordings. The L4 and FS cells were modeled with the regular-spiking neuron and FS cell described by Pospichil et al. (2008) and had parameters modified to match our recorded neurons. See Table 1 for list of model cellular parameters. To ensure that the findings of this study are not the result of the idiosyncrasies of a select group of neurons, key parameters were estimated across 30 recorded neurons (10 from each: TC, TRN, and L4) and are shown in Table 2.

The model contains an input stream representing sensory afferents to the TC cell (e.g., optic tract input to the visual thalamus), here referred to as "afferent" stimulation. In the nonreciprocal network, the TRN received synaptic input that was independent of afferent input to the TC cell. The initial parameters for our synapses were derived from the following publications: retinogeniculate (Chen and Regehr 2003), thalamocortical (Laurent et al. 2002), reticulothalamic (Wanaverbecq et al. 2008), and thalamoreticular (Gentet and Ulrich 2003). The synapse derived from a hypothetical remote source (e.g., the amygdala, nonsensory cortex, basal forebrain) to the TRN was modeled as a generic excitatory synapse with mild paired-pulse depression (recovery time constant = 40 ms). It is recognized that very little is currently known about such synapses, and the neurotransmitters used likely differ in different projections (e.g., acetylcholine or GABA from the basal forebrain; Asanuma and Porter 1990; Bickford et al. 1994; Pita-Almenar et al. 2014; Sun et al. 2013), likely glutamate from the cortex since this is used in other corticoreticular (Gentet and Ulrich 2004) and corticothalamic (Kao and Coulter 1997; Turner and Salt 1998) projections. For this reason we explored a range of synaptic strengths for this synapse spanning two orders of magnitude and examined the effect of these strengths on model behavior (see Fig. 8*D*). As more is learned about the myriad pathways that impinge upon the TRN, this model may be refined. Several other parameters were systematically varied to explore their impact on network behavior. All external inputs to the TC and TRN cells were either trains of pulses at a fixed rate or Poisson-modulated pulse trains comprising individual pulses lasting one time step (0.1 ms).

Table 1. *Model cellular parameters*

TC cell	
Leak conductance	3.263 nS
Leak equilibrium potential	−60.03 mV
Fast sodium conductance	1,500 nS
Sodium equilibrium potential	50 mV
Potassium conductance	520 nS
Potassium equilibrium potential	−100 mV
T-current amplitude	45 nS
Calcium equilibrium potential	120 mV
H-current amplitude	0.608 nS
H-current equilibrium potential	−33 mV
L4 cell	
Leak conductance	4.8128 nS
Leak equilibrium potential	−60.2354 mV
Fast sodium conductance	3,000 nS
Sodium equilibrium potential	50 mV
Potassium conductance	140 nS
Potassium equilibrium potential	−90 mV
M-current amplitude	1.5 nS
TRN cell	
Leak conductance	3.7928 nS
Leak equilibrium potential	−57 mV
Fast sodium conductance	3,000 nS
Sodium equilibrium potential	50 mV
Potassium conductance	400 nS
Potassium equilibrium potential	−100 mV
T-current amplitude	21 nS
H-current amplitude	0.0192 nS
H-current equilibrium potential	−33 mV
KS-current amplitude	3.5 nS
KS current τ	200 ms
FS cell	
Leak conductance	8.252 nS
Leak equilibrium potential	−76 mV
Fast sodium conductance	300 nS
Sodium equilibrium potential	50 mV
Potassium conductance	1,100 nS
Potassium equilibrium potential	−100 mV
H-current amplitude	0 nS

TC, thalamocortical; TRN, thalamic reticular nucleus; FS, fast spiking; L4, layer 4; KS current, slow-inactivating potassium current; τ, time constant.

Table 2. *Averaged parameter estimates from 10 cells in each class (TC, TRN, and L4)*

TC cell	
Leak conductance	3.09 (0.91) nS
Leak equilibrium potential	−57.4 (9.0) mV
T-current amplitude	49.1 (11.0) nS
H-current amplitude	0.94 (0.57) nS
L4 cell	
Leak conductance	5.24 (2.33) nS
Leak equilibrium potential	−64.7 (9.6) mV
M-current amplitude	1.06 (0.58) nS
TRN cell	
Leak conductance	4.80 (1.49) nS
Leak equilibrium potential	−53.6 (3.9) mV
T-current amplitude	24.5 (12.0) nS
H-current amplitude	0.04 (0.07) nS

Values are means (SD); $n = 10$.

The parameter space of each neuron's possible conductances is rather large, and to model neurons that are realistic, computational models were matched to recordings from TC cells, TRN cells, L4 regular-spiking cells or FS cells, described above. Matching was performed with a hybrid approach of simplex minimization (Nelder and Mead 1965) and hand parameter matching. The shape and depth of cell's depolarization were matched in a point-to-point fashion under conditions in which an external current of −100 pA was applied. Matching occurred by allowing C_m, g_L, E_L, and the conductances of both the T-type calcium channel and the H-type current to be varied by the simplex optimizer. By focusing on matching the hyperpolarization curve, a good qualitative match was achieved between our simulation posthyperpolarization calcium T current and a TC cell recorded in whole cell current clamp in the presence of TTX. The conductance of the T-type calcium channel, the firing threshold of the fast sodium channel, as well as the conductances of the sodium and potassium channels were hand adjusted to match the number of spikes contained in a tonic depolarization with 100 pA as well as the number of spikes in a burst following a −100-pA hyperpolarization. As has been done previously (Bazhenov et al. 2002), modifications of resting membrane potential of the TC cell model were accomplished by adjusting the leak current g_L. For the TRN neuron, adjustments were made in the leak potential E_L rather than g_L, because changes made in g_L to depolarize cells were countered by the KS current.

All synapses were modeled using the depressing synapse model of Tsodyks and Markram (1997). This model assumes a finite number of resources that are in an active, inactive, or recovered state. These resources can be thought of as vesicles filled with neurotransmitter. Action potentials activate a set fraction U_{SE} of the available recovered resources to the active state, which then transition to an inactive state with a linear time constant τ_{inact}. The inactive resources then recover with a time constant τ_{recov}. To have realistic models of each synapse in our simulation, we used simplex minimization (described above) to select optimal parameters to matched published data of inhibitory

postsynaptic currents (IPSCs), excitatory postsynaptic potentials (EPSPs), or excitatory postsynaptic currents (EPSCs) of our respective synapses (see Table 3 for listing of synaptic parameters).

Mutual information calculations. Mutual information (MI) between the afferent spike train to the TC neuron and the output spike train measured at the L4 cortical neuron was evaluated with an MI estimator:

$$\mathrm{MI} = \sum_{i}^{M}\sum_{j}^{M} P_{ij}^{out,in}\log_2\frac{P_{ij}^{out,in}}{P_i^{out}P_j^{in}}$$

Where $P_{ij}^{\text{out, in}}$ is the joint probability of an input event and an output event (both defined below), P_j^{in} is the marginal probability of an input event, P_i^{out} is the marginal probability of an output event, i = bin number (when using the output marginal probability), j = bin number (when using the input marginal probability) and M = total number of bins.

The uniform partition to compute MI does not work well for processes with incomparable timescales (Darbellay and Vajda 1999; Marek and Tichavsky 2008). Therefore, because of significant differences in L4 firing rates observed across different afferent input rates, a variant of the adaptive partition (Cellucci et al. 2005) has been applied. The partitioning used here relies on output spike intervals to take into account different rates of L4 output spikes observed with different rates of afferent input spikes. If a uniform partition had been used, the different rates of L4 output spikes would have created a different resolution of analysis for each afferent input rate, confounding comparisons across afferent input rates.

Input events were defined as being the spikes from the afferent input to the TC cell (i.e., spikes in an optic tract axon). For each output interval Δt_i^{out}, these inputs were represented as the number of spikes n_i. N is defined as the total number of input spikes on the whole time series. Therefore, the marginal probability of an input event was defined as

$$P_i^{in} = \frac{n_i}{N}$$

Output events were defined as the intervals between spikes in the L4 neuron. Therefore, the marginal probability of an output event was defined as

$$P_i^{out} = \frac{\Delta t_i^{out}}{T}$$

where T = total simulation time.

The joint probability $P^{\text{out, in}}$ for any combination of n_i and Δt_i^{out} was calculated by constructing a two-dimensional matrix with output interval bins on the horizontal axis and input spike number in each bin on the vertical axis. Entries on the diagonal of the matrix all equal $1/N$. Off-diagonal entries equal either zero for unique combinations of n_i and Δt_i^{out} or $1/N$ for repeated values of n_i for a given Δt_i^{out}. Therefore, for any input-output sequences that were highly predictable (i.e., a similar number of input spikes for every output interval), $P^{\text{out, in}}$ was maximized. For uncorrelated input-output sequences, most off-diagonal entries to the matrix were 0, minimizing $P^{\text{out, in}}$.

The simulations were all coded in MATLAB. All time integration was accomplished with a hybrid analytic-numerical integration scheme proposed by Moore and Ramon (1974), which provides numerically accurate solutions to Hodgkin-Huxley models while maintaining a reasonable computational cost. All simulations were run on a Dell XPS machine using a Windows operating system. Thalamocortical transfer functions were plotted as L4 spike output (y-axis) vs. afferent stimulation rate (x-axis). Bandwidth was computed by using the standard deviation of a Gaussian function fitted to the transfer function (with GraphPad software).

Table 3. *Model synaptic parameters*

External synapse to TC cell	
Conductance	32 nS
τ_{recov}	125 ms
τ_{inact}	2.64 ms
Equilibrium potential	0 mV
U_{SE}	0.76
External synapse to TRN cell	
Conductance	32 nS
τ_{recov}	40 ms
τ_{inact}	10.58 ms
Equilibrium potential	0 mV
U_{SE}	0.3
TRN-to-TC cell synapse	
Conductance	80 nS
τ_{recov}	167.29 ms
τ_{inact}	16.62 ms
Equilibrium potential	−80 mV
U_{SE}	0.62
TC-to-TRN cell synapse	
Conductance	150 nS
τ_{recov}	500 ms
τ_{inact}	2.64 ms
Equilibrium potential	0 mV
U_{SE}	0.76
TC-to-L4 or FS synapse	
Conductance	50 nS
τ_{recov}	160 ms
τ_{inact}	11.52 ms
Equilibrium potential	0 mV
U_{SE}	0.8113
FS-to-L4 synapse	
Conductance	50 nS
τ_{recov}	511.41 ms
τ_{inact}	7.162 ms
Equilibrium potential	−100 mV
U_{SE}	0.2

τ_{recov}, τ_{inact}, time constants of recovery, transition to inactive state; U_{SE}, set fraction of available recovered resources to active state.

RESULTS

Model comparison to physiological data. Consistent with many previous reports (Jahnsen and Llinas 1984; Jones 2007; Sherman 2001), depolarization of a real thalamic neuron from its resting potential leads to trains of individual action potentials, with firing rates that are dependent on the degree of depolarization and with rates that show minimal adaptation over time (Fig. 1*B*). Hyperpolarization of the same cell leads to a delayed drift of depolarization that is most apparent toward the end of the hyperpolarizing current pulse. This depolarizing drift is likely a consequence of an underlying hyperpolarization-activated cation current (a.k.a. the sag current), known to exist in TC neurons (Lüthi and McCormick 1998). This depolarization drift is followed by a rebound slow potential with a burst of fast action potentials riding on top of the slow potential (i.e., the "burst"; Fig. 1*B*). Similar to the real thalamic neuron, and previous reports with a similar model (Deleuze et al. 2012; Destexhe et al. 1998), our model thalamic neuron also fired trains of individual action potentials when depolarized, showed a sag current late during hyperpolarization, and had a burst of fast action potentials riding a slow depolarization after the injection of negative current (Fig. 1*C*). Modeled TRN neurons also showed bursting after hyperpolarization, as seen in real TRN neurons (Fig. 1, *D* and *E*; Huguenard and Prince 1992), and voltage traces from modeled cortical L4 cells closely approximated the voltage traces and firing properties of real regular-spiking neurons (Fig. 1, *F* and *G*).

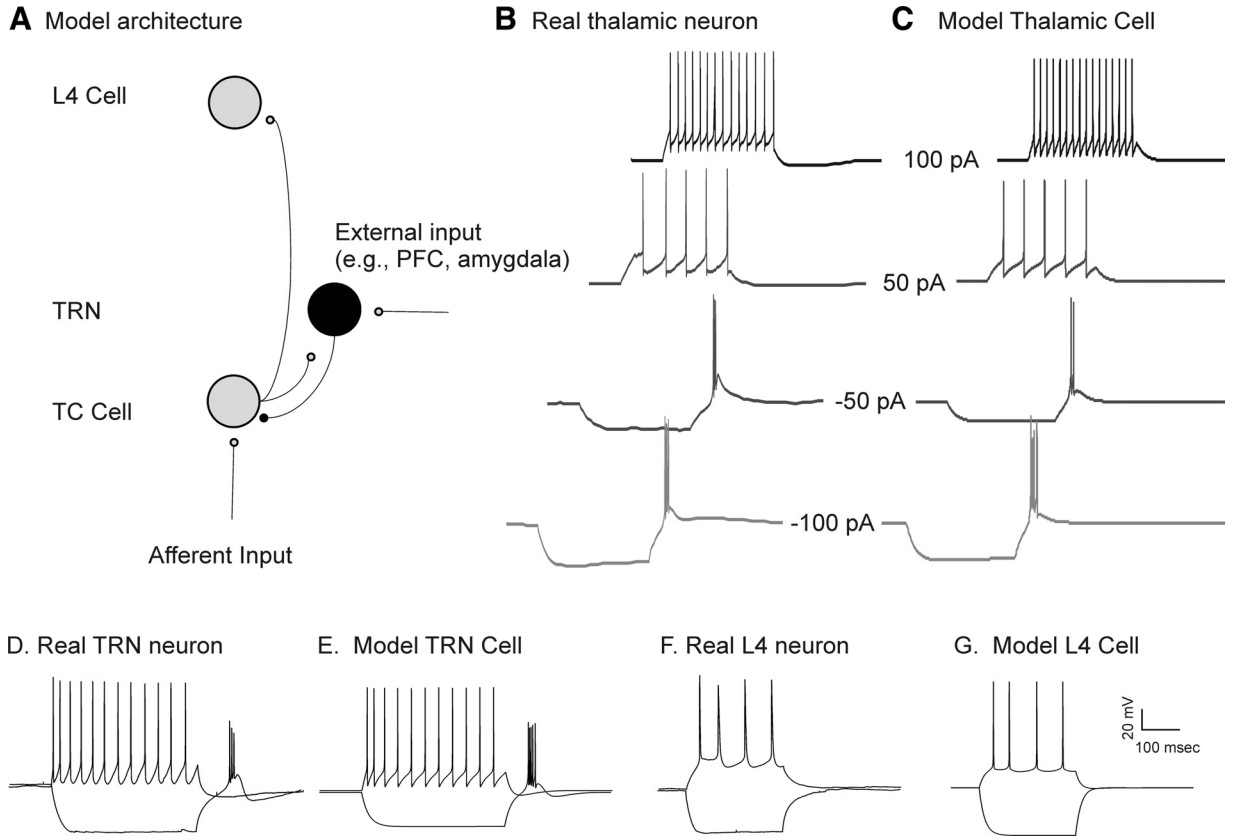

Fig. 1. *A*: model architecture. Independent Poisson inputs are fed into a thalamocortical (TC) neuron ("afferent input") or a thalamic reticular nucleus (TRN) neuron ("external input"). The TRN may also receive inputs from a TC cell, then sends a GABAergic input to the TC cell, which projects to a layer 4 (L4) cell. PFC, prefrontal cortex. *B*: a real TC cell, recorded from the ventral posterior medial part of the thalamus in current-clamp mode, in response to direct current injections from −100 pA to +100 pA. *C*: the behavior of a model cell in response to the same inputs. *D–G*: real (*D*) and model (*E*) TRN cells and real (*F*) and model (*G*) L4 cells. See text for details.

Baseline model synaptic characteristics. Stimulation of the TC cell from sensory afferents modeled after a retinogeniculate synapse with high synaptic efficacy and strong synaptic depression (i.e., a "driver synapse"; Reichova and Sherman 2004) showed significant rate-dependent effects. Stimulation of afferents at rates of 5 or 10 Hz produced a single postsynaptic action potential for each incoming action potential. At 20 Hz, only the initial incoming action potentials are transmitted through this synapse (Fig. 2*A*). Similarly, the TC synapse was modeled as a high-efficacy, high-synaptic depression synapse and therefore also showed loss of temporal fidelity at synaptic stimulation rates above 10 Hz (Fig. 2*B*). A range of different time constants and magnitudes of synaptic depression for both of these synapses has been reported in the literature and used

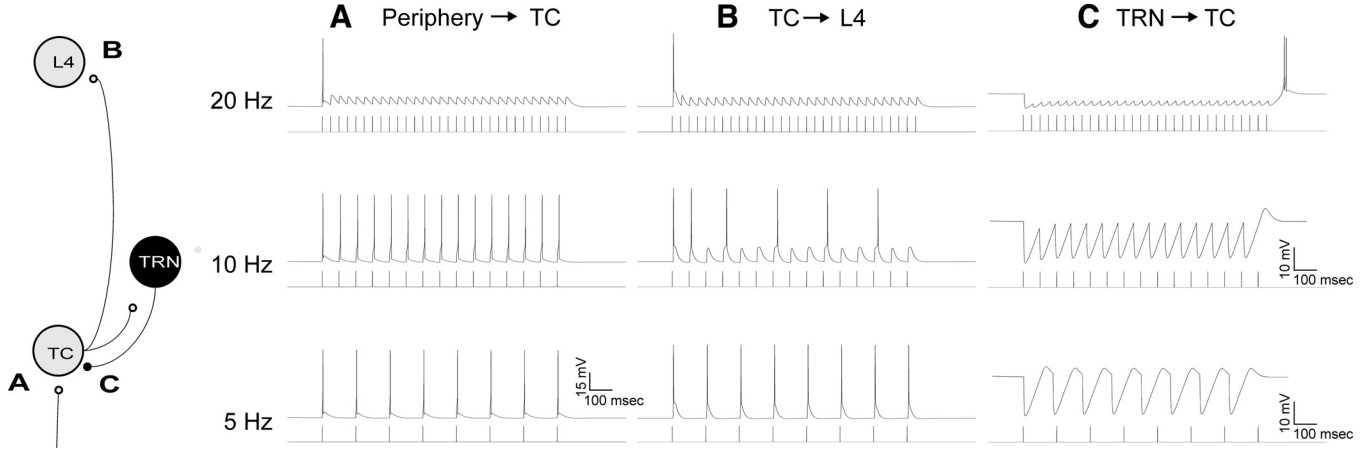

Fig. 2. Illustration of the behavior of the 3 main synapses in this model as they are driven at 5 Hz, 10 Hz and 20 Hz. *A*: the afferent synapse to the TC is driven at different rates, showing depression at rates > 10 Hz. *B*: the TC-to-L4 synapse is driven at different rates, directly by simulating stimulation of the TC axon, showing depression at rates > 10 Hz. *C*: the TRN-to-TC synapse is driven at different rates, showing hyperpolarization with rebound depolarizations, driven by T currents, which culminate in rebound spikes at rates above 10 Hz. Note that all *y*-axes use a 15-mV marker except the bottom 2 nonspiking traces in *C*, which have an expanded *y*-axis to illustrate subthreshold dynamics.

in previous modeling studies (Banitt et al. 2007; Bartlett and Smith 2002; Boudreau and Ferster 2005; Chance et al. 1998; Chen and Regehr 2003; Chung et al. 2002; Laurent et al. 2002; Reig et al. 2006; Wehr and Zador 2005), and the impact of systematically modifying these time constants is explored below. Stimulation of the TRN-to-TC synapse at low rates produces a hyperpolarization of the TC cell, followed by a rebound depolarization without spiking. As the rate of TRN stimulation is increased, the degree of synaptic depression became more evident, and the magnitude of the rebound depolarizing current increases, culminating in a two-spike rebound burst with stimulation rates of 20 Hz and above (Fig. 2*C*).

The impact of incorporation of the TRN, initially in a closed-loop configuration, was examined to determine whether our model shows behavior similar to previous modeling studies (Destexhe et al. 1993, 1996; Steriade et al. 1993a). As expected, in response to a 2-s-long tonic afferent input (modeled as a train of afferent spikes at 1,000 Hz), the TC and TRN neurons fire alternately at ~11 Hz. The oscillatory firing of the TC cell elicits rhythmic spikes in the L4 cell. The oscillations cease at the termination of the stimulus because of the absence of excitatory drive to the TC cell (Fig. 3).

Behavior of the open-loop network. The behavior of the open-loop network using independent Poisson-modulated trains of pulses as inputs to the TC and TRN cells was examined. In the absence of TRN input (Fig. 4*A*), Poisson-modulated input at an average rate of 25 Hz produced a spike train of ~3.1 spikes/s in the TC cell and 2.8 spikes/s in the L4 cell. The L4 cell responded to most of the TC spikes with a spike unless TC spikes came in rapid succession, which were filtered out by the paired pulse depression built into the TC synapse model (Fig. 4*A*). The interspike interval histogram of the TC cell shows a single peak at ~150 ms, with a long tail of intervals extending out to ~900 ms.

When input to the TRN is added, the behavior of the circuit changes. Figure 4*B* illustrates the results when the TRN received Poisson-modulated inputs at an average rate of 5 Hz while the TC cell continued to receive inputs at an average rate of 25 Hz, in response to an afferent stimulus identical to that used for the simulation in Fig. 4*A*. In the presence of inputs to the TRN, TC cells fire a mixture of individual spikes and bursts (Fig. 4*B*). The total spike rate in the TC cell was 5.6 spikes/s, which is ~81% higher than without the TRN, while the total spike rate of the L4 cell was 4.4 spikes/s, which is ~57% higher than the spike rate without the TRN. It is notable that bursts are seen infrequently in the TC cell but still produce substantial enhancement of L4 spiking. In addition, the convergence of postinhibitory depolarizations and direct excitatory afferent inputs allows several spikes to appear in the L4 cell that were not apparent without activation of the TRN (Fig. 4*B*). Other L4 spikes shifted their timing compared with the original stimulus without the TRN (Fig. 4*B*). Similar to in vivo data from the thalamus of awake subjects (Jeanmonod et al. 1996; Ramcharan et al. 2000), the interspike interval histogram of the TC cell shows two peaks: one corresponding to the action potentials within the bursts (~6 ms) and the other corresponding to action potentials between bursts (~150 ms). These data suggest that the presence of the TRN in an open-loop configuration may increase TC and L4 total spike output, that this is accomplished by changing the interval statistics of the TC spike train, and that the increase in L4 output is not solely dependent upon TC cell bursting, which is seen very infrequently in this example (~0.5 Hz, compared with a total spike rate of 5.6 Hz).

Different input rates to both TC and TRN cells were explored, ranging in average rate from 0.5 Hz to 200 Hz, with rates being logarithmically spaced. All inputs to TC and TRN cells were Poisson distributed. Without TRN stimulation, both TC and L4 cells demonstrated incremental increases in firing rate as the average afferent input rate increased up to ~10 Hz, and at higher rates a decrease in firing rates was observed (first column in Fig. 5*A* and black line in Fig. 5*B*). The drop-off in spiking with low and high rates is caused by different factors. With low afferent stimulation rates, the low spiking rates are related to the small numbers of input pulses provided to these cells. As the rate of afferent stimulation increased, the spike outputs increased until synaptic depression diminished postsynaptic firing at each synapse (recovery time constant $\tau = 125$ ms for each synapse in the baseline model). At rates > 10 Hz, the drop-off in spiking is related to synaptic depression. This point is made more clear as the value of τ is varied at the afferent and TC synapses (see below).

Particular combinations of input rates to the TRN cell and to the TC cell produced a maximum total spike output in the L4 cell (Fig. 5*A*), showing a peak response when the average rates of input to both the TRN cell and the TC cell were each ~10 Hz. The presence of input to the TRN altered the filtering properties of L4 neurons in complex ways (Fig. 5, *B–F*). The bandwidth of the thalamocortical transfer functions measured at the L4 neuron was ~35 Hz. As the rate of input to the TRN increased, the thalamocortical transfer function initially broadened, with bandwidths approaching 60 Hz at afferent rates between 5 and 50 Hz, and then narrowed again, with bandwidths returning to ~35 Hz at TRN rates of 200 Hz. These data suggest that the TRN adjusts the tuning properties of the thalamocortical filter.

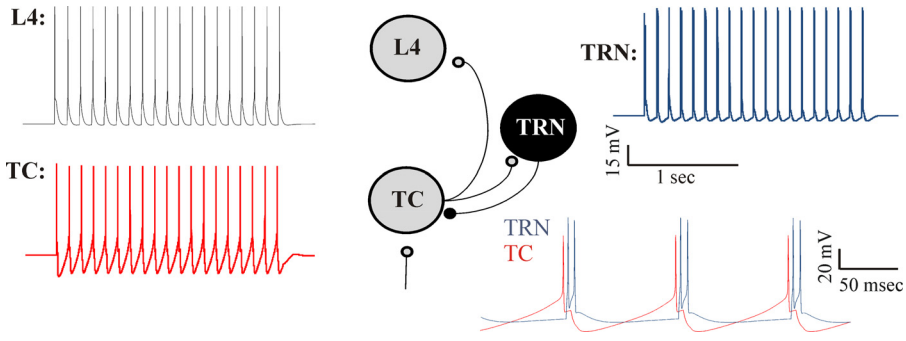

Fig. 3. Behavior of the reciprocal model. Tonic input to the TC cell produces rhythmic spiking at ~10 Hz in the TC cell (red) and the TRN cell (blue) and an onset response in the L4 neuron (black). *Inset*, *bottom right*, shows higher-resolution view of TC and TRN cell activity.

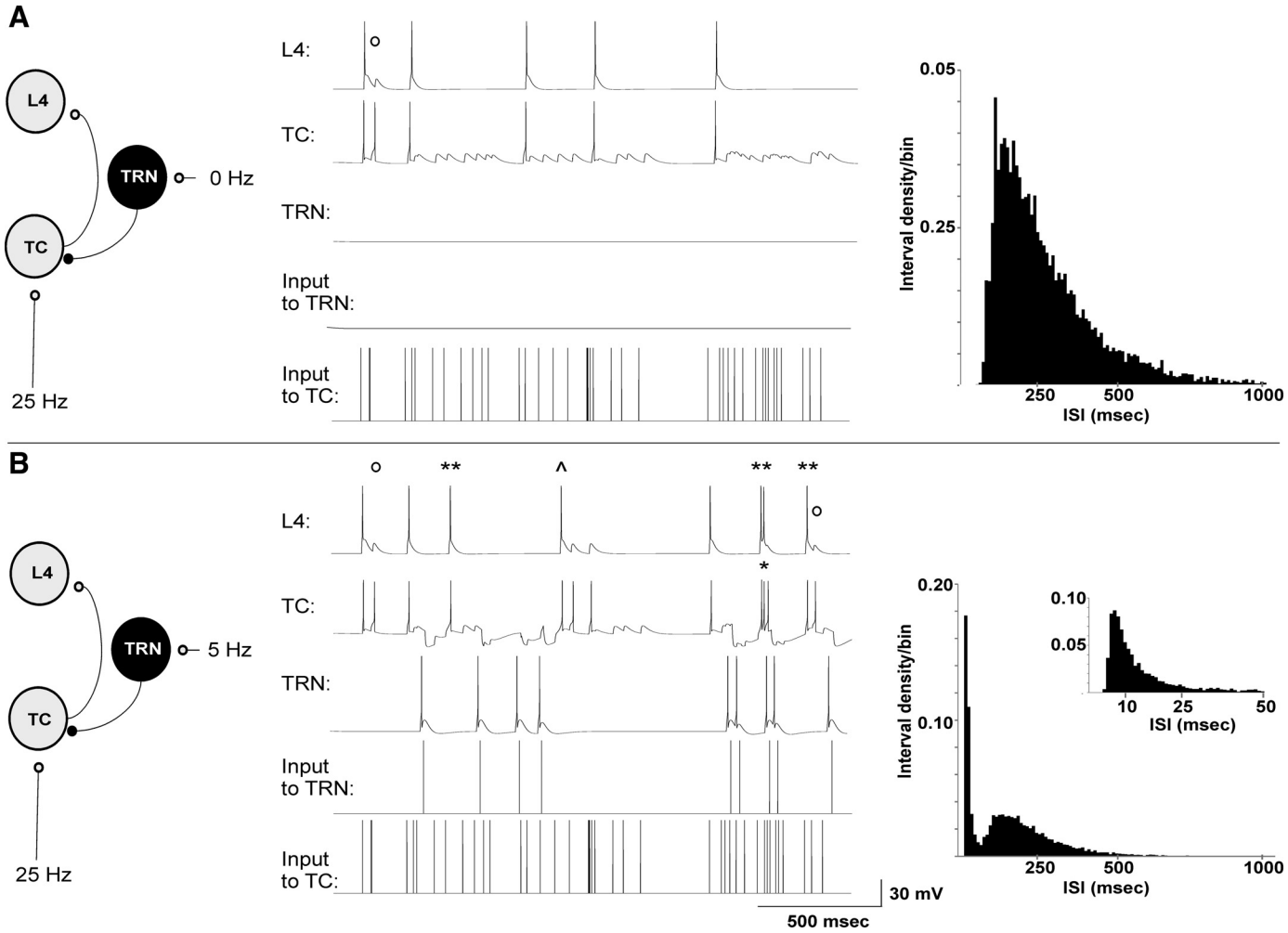

Fig. 4. Illustration of the impact of the TRN on a TC and a L4 cell while there is concurrent afferent input to the TC cell. *A*: with no input to the TRN but input to the TC cell of a 25 Hz-modulated pulse train, the TC cell fires intermittent spikes and drives the L4 cell, with occasional failures at the TC synapse due to TC synaptic depression (open circle). Interspike interval (ISI) histogram (*right*) shows a single peak at ~150 ms. *B*: with inclusion of TRN input at 5 Hz and an external stimulus to TC cells identical to that in *A*, TC cells show occasional bursts (single asterisk), but mostly individual spikes, leading to a greater total number of spikes at the L4 cell (double asterisk for spikes seen in the L4 cell seen only when TRN is receiving input). Other L4 spikes shifted their timing relative to the case prior to engaging the TRN (caret). Interspike interval histograms from the TC cell show 2 peaks, 1 corresponding to the interburst interval at ~150 ms and another corresponding to the spikes within the bursts, peaking at ~6 ms (shown in *inset*).

To further examine the impact of the TRN on L4 firing rates, a normalized spike output matrix was constructed by subtracting the baseline firing rates (without the TRN, which is the first column of Fig. 5*A*) from the corresponding firing rates when the TRN was being stimulated (Fig. 5*D*). This difference matrix, shown as a three-dimensional contour plot, illustrates that most of the TRN-induced enhancement in L4 output was seen at the highest rates of afferent stimulation, which is due to recovery from synaptic depression in the TC cell, as shown in Fig. 4*B*. The greatest suppression of L4 output, shown as a negative-going wave with an arrow, is seen at the highest rates of TRN stimulation. Review of individual filter functions from Fig. 5*D* illustrate the rate-dependent enhancement and suppression phenomena more clearly. For example, normalized L4 spiking rates obtained at two different rates of TRN stimulation (25 and 150 Hz), and at varying rates of afferent input, are shown in Fig. 5*E*. At a rate of stimulation of the TRN of 25 Hz, maximum enhancement in L4 spiking is seen at the highest rates of afferent stimulation to the TC cell. When the stimulation rate of the TRN is raised to 150 Hz mostly suppression is seen, and this suppression is most evident when afferent stimulation to the TC cell is ~20–30 Hz. When looked at from the reverse perspective, that is, by holding the rate of afferent stimulation fixed at either 25 or 150 Hz and varying the rate of stimulation of the TRN (Fig. 5*F*), it becomes clear that the TRN is more likely to enhance L4 spiking when afferent rates are high (150 Hz) and to suppress L4 spiking when afferent rates are intermediate (25 Hz). These data illustrate the complex interrelationships between the rates of stimulation of the TRN and the TC cell and the resulting pattern of spiking at the L4 cell.

To ensure that these findings are not a result of the particular combination of parameters used from individual neurons, the simulations were rerun with averaged parameters obtained across the three cell types (10 of each cell type). These data are illustrated in Fig. 6 and show that the phenomena of rate-dependent enhancement and suppression are similar when using averaged parameters and parameters derived from individual cells (compare to Fig. 5, *A* and *D*).

Removal of T-type calcium channels substantially altered the impact of the TRN on L4 firing. In the absence of T-type

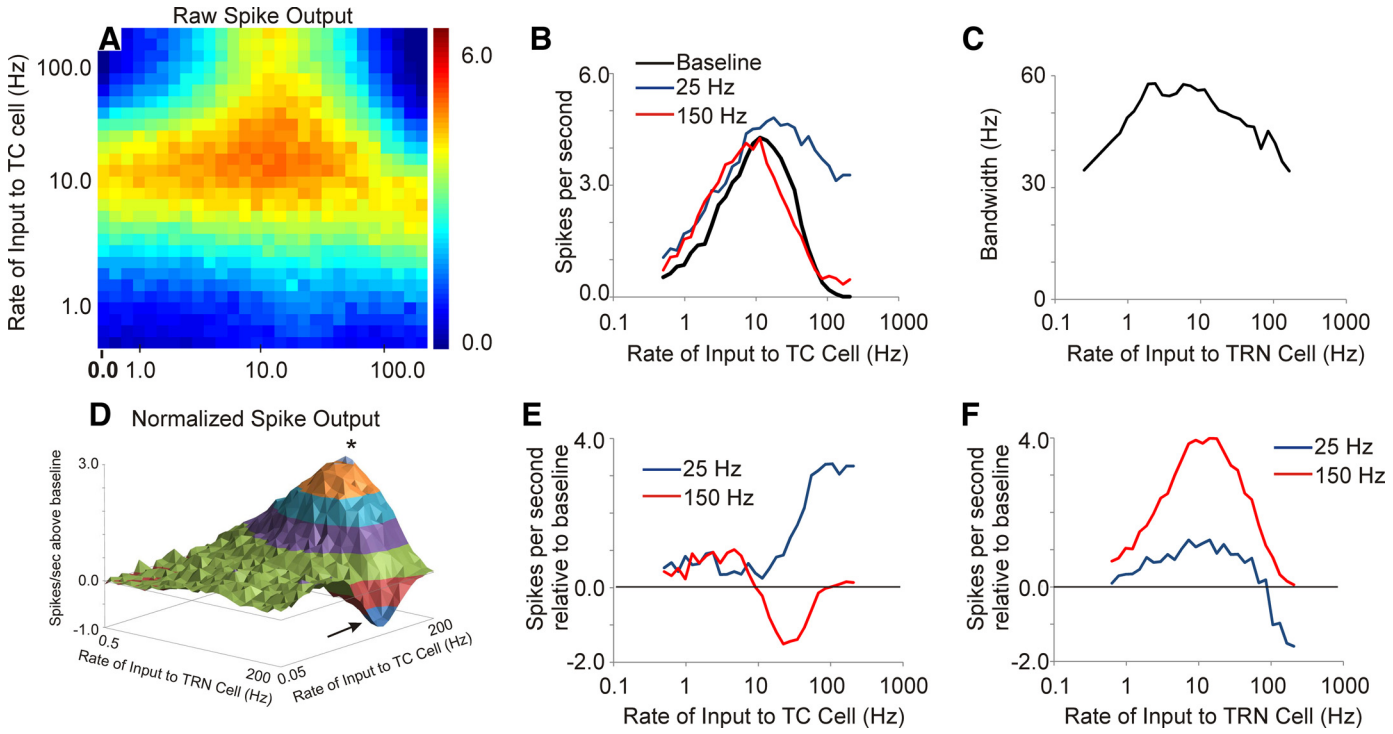

Fig. 5. Output of L4 cell in response to a range of combinations of inputs to TC and TRN cells ranging from 0.5 Hz to 200 Hz. *A*: heat map of the raw spike output in the L4 cell. *B*: thalamocortical transfer functions with no input to TRN (baseline) compared with 25-Hz input to TRN and 150-Hz input to TRN showing broadening of the transfer function. *C*: bandwidth of the thalamocortical transfer function changes as a function of TRN stimulation rate. *D*: 3-dimensional contour plot of the difference of spike output relative to the baseline case of no input to the TRN in the L4 cell. Asterisk shows area of maximal enhancement, and arrow shows area of maximal suppression. *E*: individual normalized thalamocortical transfer functions obtained at 2 different rates of TRN stimulation (25 and 150 Hz); 25 Hz produces enhancement at high rates of afferent stimulation to the TC cell, while 150 Hz produces depression of L4 spiking. *F*: individual traces showing normalized spike output as a function of TRN stimulation rate at 2 different rates of afferent stimulation (25 and 150 Hz).

calcium channels, increasing the rate of TRN stimulation monotonically reduced the spiking output of the L4 cell (Fig. 7, *A* and *B*). Unlike the changes in bandwidth seen with changing rates of TRN input in the presence of thalamic T currents seen in Fig. 5*C*, removal of T currents produced bandwidths that are initially flat and then diminish as TRN stimulation rates rise, primarily because the magnitude of the response at high TRN rates declines precipitously (Fig. 7*C*). These data suggest that TRN-based enhancement of spike output and adjustment of thalamocortical transfer function tuning are dependent upon thalamic T-type calcium channels.

Impact of changing synaptic and biophysical parameters. The effects of changing several synaptic and biophysical properties on the magnitude of TRN-based enhancement in L4 spiking rates were explored. During these parameter changes, all other biophysical and synaptic properties were held constant. TRN-based enhancement of L4 spiking rates was found to be highly dependent on the magnitude of the T-type calcium current (Fig. 8*A*). Enhancement of L4 output was seen at T-type channel conductance values as low as 15 nS and showed a steep increase as the conductance value was increased to 30 nS. Beyond 50 nS, the increase plateaued. In addition, adjustment of the resting potential of TC and TRN neurons was done as a way to simulate the presence of typically depolarizing modulators, such as acetylcholine or norepinephrine. Mild tonic hyperpolarization of the TC cell shut down TC spiking by dropping EPSP amplitudes below spiking thresholds, while tonic depolarization gradually increased TRN-based enhancement of L4 spike output (Fig. 8*B*). This increase in enhancement is related to higher tonic spiking rates in TC neurons, which suppressed L4 spiking and was then relieved by the intermittent pauses and rebounds induced by the TRN. L4 spiking output was relatively stable across a broad range of resting potentials of TRN neurons, although at strong depolarizations (about +12 mV relative to baseline) TRN spike rates became quite high and tonically suppressed TC neurons, diminishing L4 output (Fig. 8*B*). This suppression was partially relieved by depolarizing both the TC neuron and the TRN neuron by ~12 mV (Fig. 8*B*). Changing the recovery time constant of the afferent input to the TC cell or the TC synapse from 25 ms to 800 ms did gradually diminish the magnitude of enhancement seen in the L4 cell (Fig. 8*C*), and this drop was more prominent when the TC synapse recovery time constant was increased. This suggests that synaptic filtering at either synapse is not the sole cause of TRN-based enhancement of L4 spiking. The strength of synaptic projections from external sources (such as the prefrontal cortex, amygdala, or nonreciprocal portions of the thalamus) is not yet known and may vary between these different sources of input. Therefore we examined the impact of varying the strength of the external synapse to the TRN from 2 to 256 nS (Fig. 8*D*). At low levels of synaptic conductance, there is essentially no enhancement of L4 firing, related to absence of TRN firing under these conditions. Above 10 nS, there is a sharp increase in enhancement, which drops off gradually at higher synaptic strengths. This latter result is consistent with the overall result that the degree of TRN-mediated enhancement of TC trans-

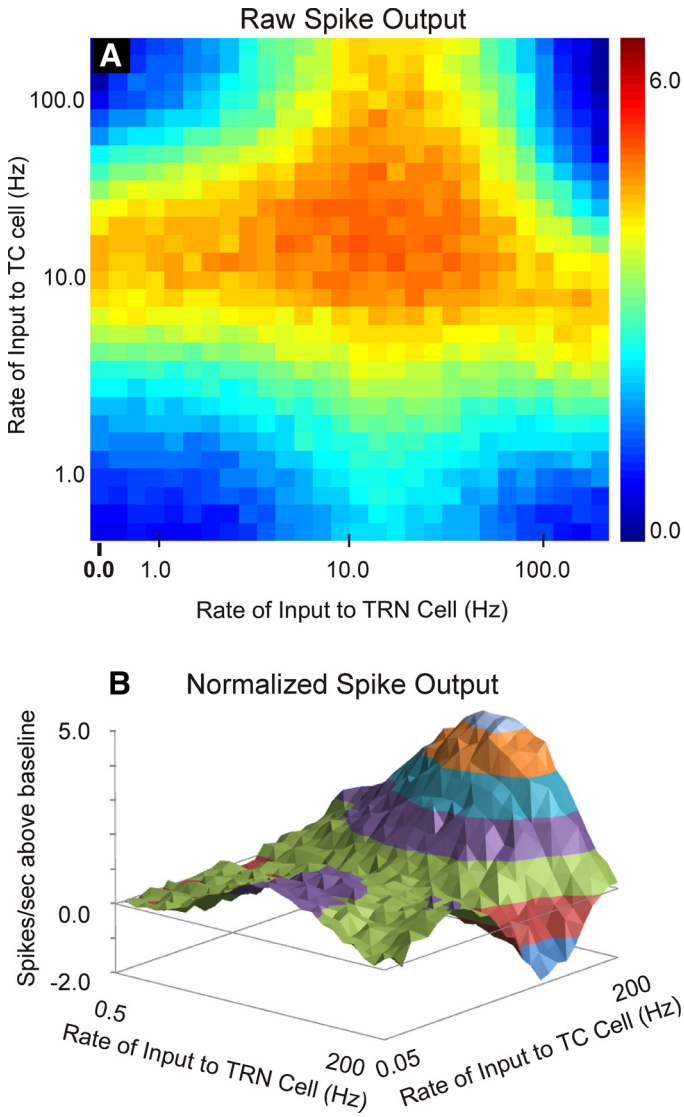

Fig. 6. Output of L4 cell in response to a range of combinations of inputs to TC and TRN cells ranging from 0.5 Hz to 200 Hz, using the averaged parameters shown in Table 2. *A*: heat map of the raw spike output in the L4 cell. *B*: 3-dimensional contour plot of the difference of spike output relative to the baseline case of no input to the TRN in the L4 cell.

mission is maximal at intermediate rates of activation of TRN neurons (as illustrated in Fig. 5*F*).

Impact of FS interneurons. TC neurons are known to make strong synapses on FS interneurons, which then provide GABAergic innervation to L4 regular-spiking neurons (Cruikshank et al. 2007; Sun et al. 2006). We therefore examined the impact of including an FS interneuron interposed between the TC cell and the L4 cell (see Fig. 9*A* for model architecture and Fig. 9, *B* and *C*, for the real and modeled FS cells, respectively). The general pattern of raw spike counts in the presence of the FS cell is generally similar to that without the FS cell (compare Fig. 9*D* to Fig. 5*A*). Two differences are that *1*) the overall spike counts are slightly diminished in the presence of the FS cell and *2*) the highest rates of TRN stimulation produce less enhancement than in the model without the FS cell (compare circled area in Fig. 9*D* to similar region in Fig. 5*A*). This is most evident when looking at the normalized spike output (Fig. 9*E*), where spike rates diminish by nearly 3 spikes/s at the highest TRN rates, while they only dropped by ~1 spike/s without the FS cell. Finally, the bandwidths of the thalamocortical transfer functions were narrower in the presence of the FS cell, particularly at high rates of TRN stimulation (Fig. 9*F*).

Impact of TRN on mutual information. Given previous work demonstrating the impact of bursting on the information content of thalamic spike trains (Reinagel et al. 1999), we examined the impact of the TRN on the relationship between the temporal pattern of afferent input to the TC cell and L4 temporal spiking patterns using MI. In the absence of the TRN, the MI rose with afferent input rate, then peaked at input rates of ~2 Hz, and then declined (Fig. 10*A*). This initial rise was likely related to the increasing number of L4 spikes produced as the number of input pulses grew, because normalizing by the number of L4 spikes produced an essentially a monotonic decreasing amount of MI as the afferent rate increased (Fig. 10*B*). In addition, normalizing by number of spikes virtually equalized the MI (expressed as bits/spike) across different simulation durations (Fig. 10*B*). At afferent stimulation rates above 2 Hz, MI diminished, related to diminishing correspondence between input and output because of adaptation.

Inclusion of the TRN had different effects on MI depending on the rate of afferent input to the TC cell. Using a value of normalized MI (normalized to number of spikes) expressed relative to the maximum MI at a particular afferent stimulation rate, the TRN caused a prominent drop in MI at TRN stimulation rates between 5 and 20 Hz and a recovery of MI above 20 Hz (Fig. 10, *C* and *D*). As TRN stimulation rate increased, this pattern appeared to invert, such that at high rates of afferent stimulation TRN stimulation rates in the 1–20 Hz range boosted MI quite considerably, then declined again at higher rates of TRN stimulation (Fig. 10, *C* and *D*). Note that these changes cannot simply be spike rate dependent since these MI values have been normalized for L4 spike rate.

DISCUSSION

In the present study, we found that model circuits that contain nonreciprocal TRN-TC connectivity can potentiate ascending signals as they pass through the thalamus. In addition, this potentiation is only seen for a restricted range of rates of stimulation of TC and TRN cells; suppression is seen at others. This suggests that the TRN, when placed in an open-loop configuration with the dorsal thalamus, can act to create a tunable temporal filter such that only particular rates of ascending information activate the cortex. In addition, this filtering capacity disappeared when T-type calcium channels were removed, suggesting that the filtering was dependent on the activation of these channels. Finally, when this model was reconfigured into a closed-loop organization, oscillatory activity at similar rates seen in spindles was observed, which is similar to many previous modeling studies. This final point suggests that the only fundamental difference between the present model and previous models is the connectivity of the dorsal thalamus and TRN cells. These data highlight the considerable importance of knowing the microarchitecture of TRN-thalamic circuitry to make inferences about larger-scale network activity.

Methodological issues. The models in the present study are, by design, extremely simple and do not capture the wealth of

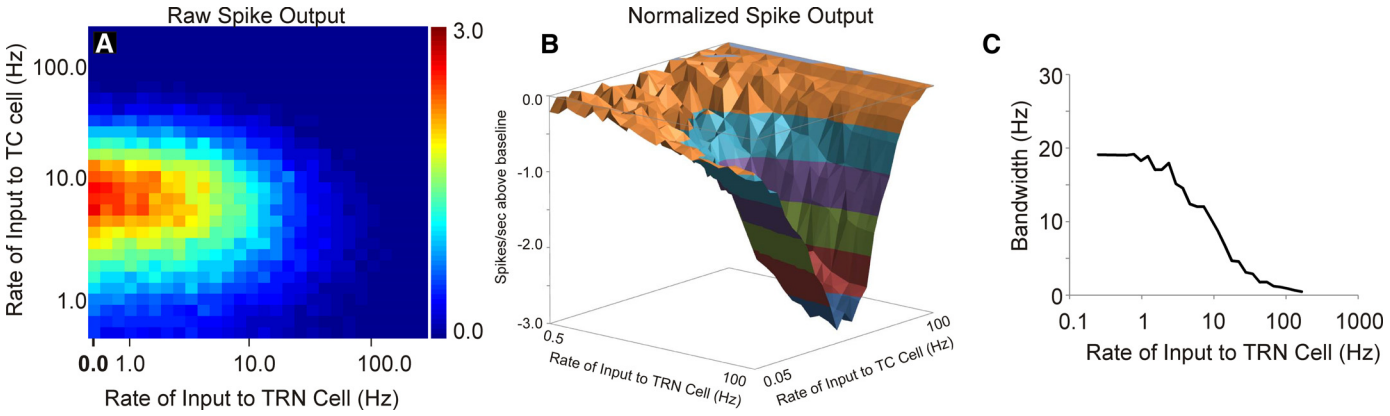

Fig. 7. Impact of removal of the T current on model behavior. Removal of the T currents diminishes all enhancement of firing seen both in the raw spike output (*A*) and the normalized spike output (*B*). The bandwidth of the thalamocortical transfer functions also decreases as a function of rate of TRN stimulation, related to the low overall spike counts at high TRN rates (*C*).

biophysical detail present in real TC, TRN, or L4 cortical thalamorecipient cells. One particular issue that may benefit from a more biophysically detailed model is the presence of T-type calcium channels on dendrites (Crandall et al. 2010). An assumption of the present model is that ascending sensory inputs and TRN inputs are integrated at the same location, although it is certainly possible that these inputs may be physically separated to different parts of the dendritic tree or to different dendrites, producing local dendritic integration. Other details have also been left out, such as cross-channel interactions in the dorsal thalamus, potentially mediated by the TRN (Crabtree and Isaac 2002; Deschênes et al. 1985; Landisman et al. 2002; Pinault and Deschênes 1998). Furthermore, there are other sources of GABAergic input onto sensory TC cells: intrinsic GABAergic interneurons (Sherman 2004), inhibition from the zona incerta (Barthó et al. 2002), or, in the case of the auditory and visual systems, ascending inhibition from the midbrain (Cucchiaro et al. 1991; Llano et al. 2014; Peruzzi et al. 1997; Venkataraman and Bartlett 2013; Winer et al. 1996). Additionally, it is not known whether such TRN-based enhancement of cortical activation would be modified by other inputs to the TRN, such as those from layer 6 of the cortex (Liu and Jones 1999). It is well recognized that corticothalamic projections can have dominant roles in the firing of thalamic neurons (Alitto and Usrey 2003; Sillito et al. 2006; Suga and Ma 2003) and that these roles may vary dynamically (Crandall et al. 2015). Since our goal was to examine the potential for the reticulothalamic pathway to modify signals ascending through the thalamus, we have not included these projections, although they may be incorporated in future simulations. In addition, excitatory synapses in this model were all relatively generic, most closely resembling AMPA-type receptors, although it is known that NMDA receptors are present on multiple modeled synapses (Funke et al. 1991; Gentet and Ulrich 2004; Gil and Amitai 1996). The impact of inclusion of NMDA currents in the present model is not yet known: enhancement of TC firing may have been seen with high afferent rates, but this may be offset by TC synaptic filtering. A dedicated exploration of the impact of NMDA currents would require systematic exploration of their impact at multiple synapses, and may easily be incorporated in future studies. Finally, L4 cells receive a number of thalamic inputs (Alonso et al. 2001; Miller et al. 2001), and synchronous firing in multiple thalamic cells may be required to produce a postsynaptic response (Bruno and Sakmann 2006). Therefore, the impact of a TRN impulse on the likelihood that an L4 neuron would fire may be dependent on TRN effects on a population of TC neurons, not just one neuron as presently modeled.

Three points should be made with respect to the validity of using the simple models used in the present study to infer network dynamics. First, all of the physiological parameters used to construct this model were obtained from recordings made at the soma, such that these values were obtained after dendritic filtering took place. Second, simple single-compartment models have been used successfully to gain insight into neural network properties, despite drastic simplifications made for the sake of tractability (Ching et al. 2010; Destexhe et al. 1993; Grillner et al. 1988). Third, now that the core behavior of this simple network has been characterized in silico, it would be straightforward to incorporate more components to the model, such as dendritic currents, cross-channel integration,

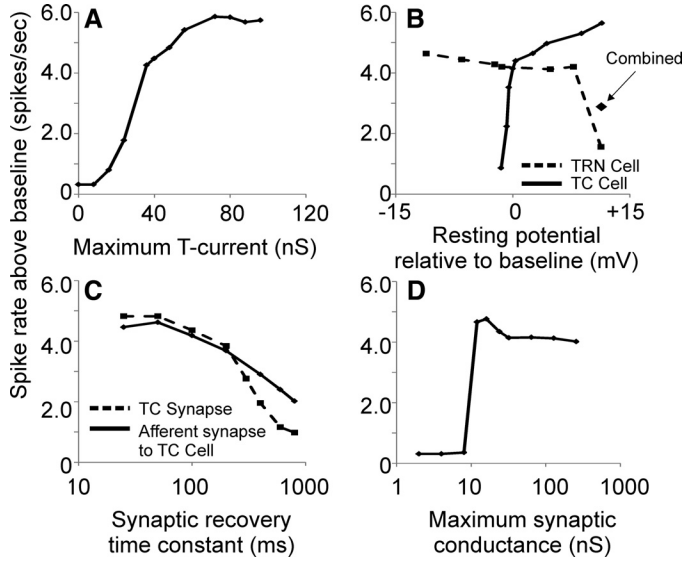

Fig. 8. Assessment of the impact of adjustment of T-current magnitude (*A*), TC and TRN cell resting membrane potential relative to the resting potential in the baseline model (*B*), afferent and TC synaptic recovery time constant (*C*), and strength of external synapse to TRN (*D*). Output is expressed as maximum spikes per second above baseline (i.e., compared with spike output at same TC stimulation rate without input to the TRN cell).

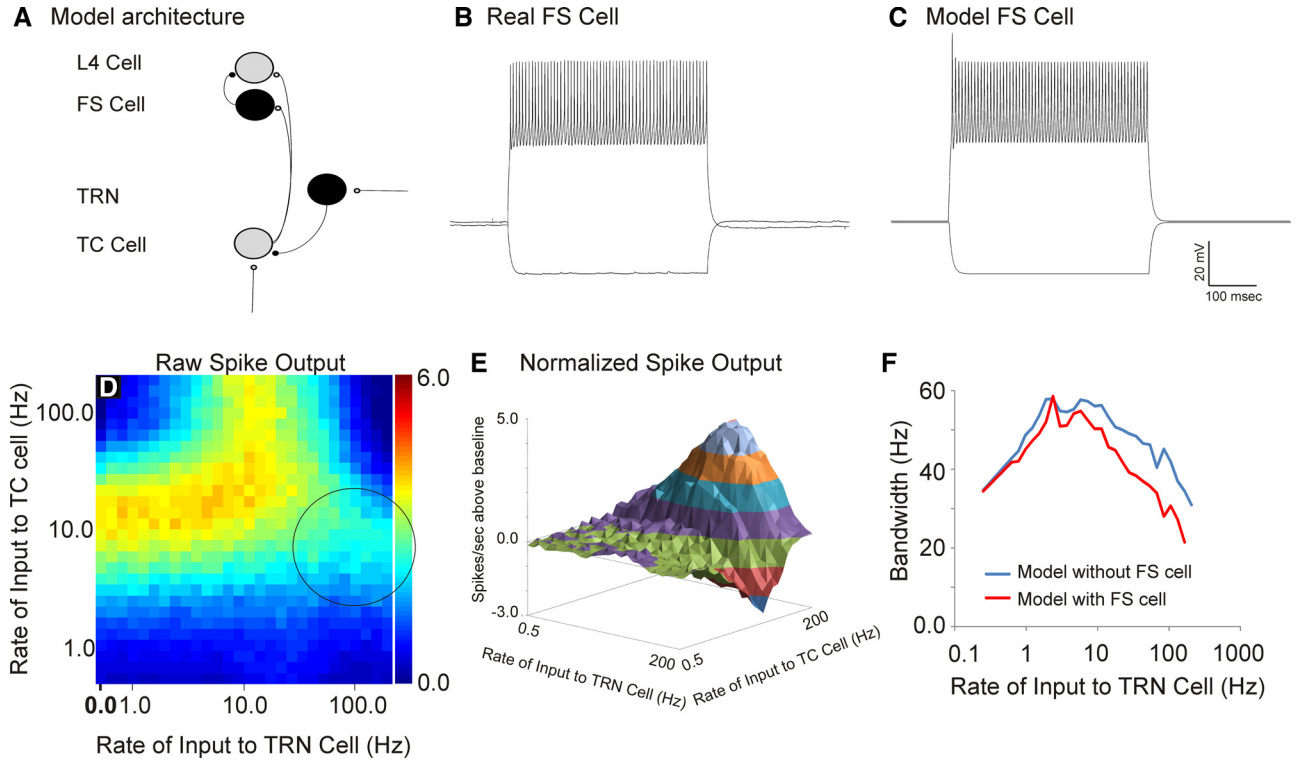

Fig. 9. Assessment of the impact of incorporation of a fast-spiking (FS cell). *A*: model architecture with FS cell interposed between a TC and a L4 cell. *B* and *C*: a real (*B*) and a model (*C*) FS cell. *D*: heat map of raw spike output at various rates of afferent and TRN stimulation showing a peak of spike outputs at TRN rates about 10 Hz and afferent rates of between 10 and 40 Hz. Circle denotes area that shows substantially less spiking than the case without the FS cell (compare to Fig. 5*A*). *E*: 3-dimensional contour plot showing normalized spike outputs with varying rates of afferent and TRN input. *F*: bandwidths of thalamocortical transfer functions in the baseline model (without the FS cell) compared with the model with the FS cell.

other forms of GABAergic input, etc., and assess their impact on model performance.

Comparison with physiological data. The present results are consistent with previous data showing the enhanced efficacy, in terms of spiking at the level of the cortex (Swadlow and Gusev 2001), detection of sensory signals (Guido et al. 1995) and information content (Reinagel et al. 1999) of thalamic neurons in burst mode. The present results also indicate that the impact of TRN modulation on both cortical spiking and MI between afferent input to the TC cell and spiking in an L4 cell is strongly dependent on the rate of stimulation of the afferent synapse to the TC neuron. For example, Fig. 5, *D* and *F*, show that potentiation of L4 activation is seen primarily only at high (>20 Hz) rates of afferent input and that at intermediate rates depression is seen. Similarly, TRN-based enhancement of MI is diminished at low afferent rates but enhanced at high afferent stimulation rates, and these changes are seen only at intermediate rates of TRN stimulation (Fig. 10, *C* and *D*). Afferent inputs to the traditional sensory parts of the thalamus, such as the lateral geniculate nucleus, medial geniculate body, and ventral posterior nucleus, are derived from the retina, inferior colliculus, and medial lemniscus/spinothalamic system, respectively. The rates of firing of thalamic-projecting neurons in these systems are highly variable, depending on the stimuli being encoded and the subsets of afferent neurons being activated, and encompass the ranges used in this study (Alitto and Usrey 2008; Davidson et al. 2007; Hubel 1960; Rose et al. 1963; Sincich et al. 2007). Given this heterogeneity of temporal patterns of afferent input to the thalamus, the present data suggest that the TRN may produce diverse effects on thalamocortical networks that strongly depend on both stimulus features as well as the spiking properties of the individual afferent projections to TC neurons.

TRN-mediated thalamocortical potentiation was sensitive to some synaptic and cellular parameters and not others. For example, adjustment of the strength of the T current strongly modulated the degree of potentiation as well as the bandwidth of the thalamocortical transfer function (Fig. 7 and Fig. 8*A*). Potentiation was seen at all T-current values above 15 nS, which encompasses T currents used across several different computational modeling studies (Deleuze et al. 2012; Destexhe et al. 1993; Pospischil et al. 2008; Wang 1994), suggesting that TRN-based enhancement of TC firing seen here is not due to selection of an artificially high value of the T current. Potentiation was also strongly diminished with increases in the afferent and TC synaptic recovery time constants. This is because high values of this time constant are suppressive for virtually all thalamic inputs. At low values of these time constants, the L4 cell tracks, spike for spike, the activity of the TC neuron. These findings, coupled with previous work showing that the degree of TC filtering can be altered by a host of different modulators and/or local network activity (Gil et al. 1997; Hirata and Castro-Alamancos 2006; Reig et al. 2006), suggest that the TC synapse may be an important point of regulation to control the response of the cortex to temporally patterned input delivered to the thalamus. Output of the L4 cell was not strongly dependent on the resting potential of the TC or TRN cell, although decreases in the degree of TRN-based enhancement of L4 spiking were seen with hyperpolarization of TC neurons or strong depolarization of TRN neurons (Fig.

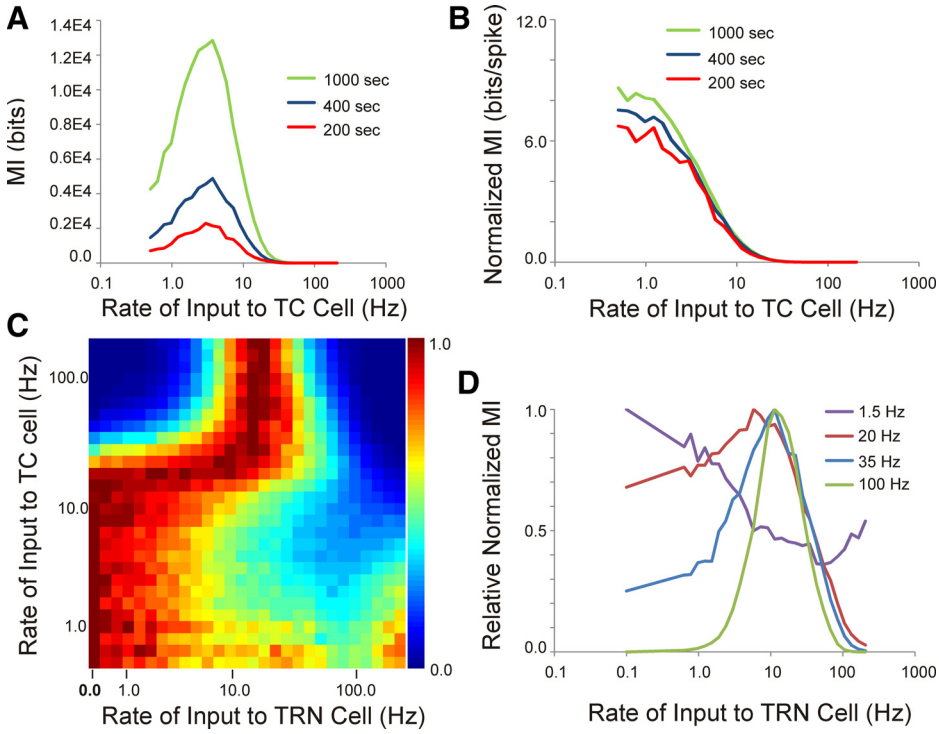

Fig. 10. Impact of the TRN on mutual information (MI). *A*: the MI between the afferent train to the TC cell and the L4 spike train increases, then decreases, as the input rate to the TC cell increases and increases as the length of the simulation increases. *B*: dividing the MI by the number of spikes in the output cell causes MI to become a monotonic decreasing function with input rate and equalizes MI across the different lengths of simulation. *C*: across a range of rates of input to the TC and TRN cell, the normalized relative MI shows a complex relationship with input rates. *D*: at low rates of afferent stimulation, TRN stimulation causes a drop in MI at low TRN rates, then a recovery of MI at higher rates. At high rates of afferent stimulation, TRN stimulation at low rates causes an increase in MI, which then decreases at high rates of TRN stimulation.

8*B*). Interestingly, the depression of L4 enhancement seen with depolarization of TRN neurons was partially recovered by also depolarizing the TC cell (Fig. 8*B*). This finding indicates that matched depolarizing input to TRN and TC neurons (such as that coming from brain stem cholinergic systems during increases in arousal) suggests that the impact of the TRN on thalamocortical activation may not be particularly state dependent.

The stimulus design needs to be considered in the interpretation of the present results. Uncorrelated Poisson-modulated pulse trains were used as simple approximations to random inputs received by the TRN and TC neuron, although it is known that many spike trains violate Poisson assumptions (Liu et al. 2001). The presence of uncorrelated inputs has implications in the MI data. For example, while it is not surprising that the addition of a source of noise, in the form of uncorrelated inputs from the TRN to the TC cell, can diminish the correspondence between the afferent input and the L4 neuron and thus diminish the MI, this drop in MI is only seen at particular combinations of rates of input to the TC and TRN cells. At high rates of input to the TC cell, the TRN causes substantial increases in the MI (see Fig. 10*D*) that cannot simply be due to an increase in L4 spiking, since MI was normalized for spike output. In this sense, the TRN can facilitate MI in a manner similar to what has been observed with stochastic resonance in other neural systems (Hänggi 2002; Stacey and Durand 2000). It is not yet known with any precision what kinds of signals are sent to the TRN from remote regions, such as the overlying cortex, prefrontal cortex, amygdala, or basal forebrain, but it is not likely that the TRN simply acts as a source of noise, since TRN spiking activity in vivo is highly correlated to sensory inputs or motor outputs (Marlinski and Beloozerova 2014; McAlonan et al. 2006; Shosaku and Sumitomo 1983; Yu et al. 2009). Future work with this model, incorporating more realistic inputs to the TRN, will be feasible once neuronal recordings in vivo from identified inputs to the TRN are available.

Bursting, inhibition, and TC coding. The idea that bursting in TC neurons may be an important form of coding information is controversial. Indeed, there is a body of literature that would suggest that bursting is seen in states of global inattention and therefore suppresses the flow of information through the thalamus. This literature is based primarily on the findings that thalamic neurons tend to hyperpolarize during sleep or drowsiness and often burst rhythmically during these states (Bereshpolova et al. 2011; Hirsch et al. 1983; Livingstone and Hubel 1981; Steriade et al. 1993b). In addition, thalamic bursting is seen during absence seizures, a state in which the organism is awake but inattentive to external stimuli (von Krosigk et al. 1993). This has led to the most common description of thalamic function, that of being a relay, which is gated based on overall states of arousal. More specifically, during drowsiness or sleep there is a decrease in activity of monaminergic afferents from the brain stem, which permits hyperpolarization of the thalamus and therefore blocks relay of information to the cortex. Then, during states of arousal, TC neurons become depolarized from the action of monoaminergic brain stem afferents and the neurons switch from burst to tonic mode and relay information with high fidelity to the cortex.

Unfortunately, this simple model of thalamic function does not account for other findings in the literature, such as the presence of bursting seen in awake animals (Fanselow et al. 2001; Guido and Weyand 1995; Ramcharan et al. 2005). In addition, several groups have found that bursts can selectively encode sensory features. For example, bursting in visual thalamic neurons robustly encodes certain types of temporal sequences, such as the movement of an object into the visual field (Lesica et al. 2006; Lesica and Stanley 2004). Other studies demonstrate that viewing naturalistic movies will induce hyperpolarizations that transition visual thalamic cells to

burst mode (Wang et al. 2007). Finally, it has been shown that bursting in visual thalamic cells is driven by specific patterns of stimulation and is a highly reliable form of signaling (Alitto et al. 2005). These data, combined with the temporal filtering characteristics of the TC synapse (Chung et al. 2002; Gil et al. 1999; Stratford et al. 1996) that provide a cortical "readout" mechanism that favors bursts, suggest that bursting not only may be a viable mode of coding but also may be more potent than tonic spikes in activating the cortex. Finally, it is important to note that, similar to the findings of others (Deleuze et al. 2012), fully elaborated bursts were not necessary to produce enhanced cortical responses; rebound T current-mediated depolarizations carrying one or two spikes were sufficient to produce enhanced cortical activation (Fig. 4*B*, *center*, TC trace). Patterns of thalamic firing potentiated by T currents, but not showing bursting, would be difficult to detect with traditional means of identifying bursts in the extracellular record (Lu et al. 1992; Ramcharan et al. 2000) but would change the statistical properties of the thalamic spike train (Fig. 4*B*, *right*).

Therefore, the present findings, coupled with previous work demonstrating the presence of nonperiodic bursting during the awake state, suggest that a more nuanced view of the thalamus and bursting may be appropriate. Although spontaneous, rhythmic bursting may be associated with states of global inattention, irregular bursting may, in fact, be a mechanism by which detection of weak signals is facilitated. This implies that modulatory inputs from remote regions such as the basal forebrain, amygdala, and prefrontal cortex can alter the activation of a particular region of the cortex by dynamically modulating the state of TC neurons during wakefulness. The fact that such low-threshold detection does not appear to occur during sleep may be due to a whole host of sleep-specific factors, for example, cortical unresponsiveness during slow-wave oscillations (Watson et al. 2008) or withdrawal of monoamine neuromodulators that may hyperpolarize thalamic cells to the point that they are unable to respond to external inputs (Livingstone and Hubel 1981). Whereas substantial advances were made in the past in understanding closed-loop TRN-thalamus interactions with reduced experimental preparations that retained only thalamus-TRN connectivity (von Krosigk et al. 1993), the results presented here suggest that more complicated dynamics are invoked once afferent inputs to the thalamus are stimulated concurrently with the TRN. Therefore, in future studies it will be necessary to test the hypotheses advanced here with experimental preparations that contain a greater degree of intact circuitry between TRN, thalamus, and afferent inputs to the thalamus, either in a slice preparation (Llano et al. 2014) or with in vivo approaches that allow excitation of the TRN while monitoring an animal's behavioral state (Halassa et al. 2011).

ACKNOWLEDGMENTS

The authors thank Dr. Kush Paul for his assistance in identifying fast-spiking interneurons in our data set.

GRANTS

D. A. Llano was supported by National Institute on Deafness and Other Communication Disorders (NIDCD) Grant DC-012125, and B. J. Slater was supported by NIDCD Grant DC-013501.

The view(s) expressed herein are those of the author(s) and do not reflect the official policy or position of Brooke Army Medical Center, the U.S. Army Medical Department, the U.S. Army Office of the Surgeon General, the Department of the Air Force, the Department of the Army or the Department of Defense or the U.S. Government.

DISCLOSURES

No conflicts of interest, financial or otherwise, are declared by the author(s).

AUTHOR CONTRIBUTIONS

Author contributions: A.M.W., E.D.G., and D.A.L. conception and design of research; A.M.W., B.J.S., E.D.G., and D.A.L. performed experiments; A.M.W., B.J.S., E.D.G., and D.A.L. analyzed data; A.M.W., B.J.S., E.D.G., and D.A.L. interpreted results of experiments; A.M.W. and D.A.L. prepared figures; A.M.W., B.J.S., E.D.G., and D.A.L. drafted manuscript; A.M.W., E.D.G., and D.A.L. edited and revised manuscript; A.M.W., B.J.S., E.D.G., and D.A.L. approved final version of manuscript.

REFERENCES

Alitto HJ, Usrey WM. Corticothalamic feedback and sensory processing. *Curr Opin Neurobiol* 13: 440–445, 2003.

Alitto HJ, Usrey WM. Origin and dynamics of extraclassical suppression in the lateral geniculate nucleus of the macaque monkey. *Neuron* 57: 135–146, 2008.

Alitto HJ, Weyand TG, Usrey WM. Distinct properties of stimulus-evoked bursts in the lateral geniculate nucleus. *J Neurosci* 25: 514–523, 2005.

Alonso JM, Usrey WM, Reid RC. Rules of connectivity between geniculate cells and simple cells in cat primary visual cortex. *J Neurosci* 21: 4002–4015, 2001.

Asanuma C, Porter LL. Light and electron microscopic evidence for a GABAergic projection from the caudal basal forebrain to the thalamic reticular nucleus in rats. *J Comp Neurol* 302: 159–172, 1990.

Banitt Y, Martin KA, Segev I. A biologically realistic model of contrast invariant orientation tuning by thalamocortical synaptic depression. *J Neurosci* 27: 10230–10239, 2007.

Barthó P, Freund TF, Acsády L. Selective GABAergic innervation of thalamic nuclei from zona incerta. *Eur J Neurosci* 16: 999–1014, 2002.

Bartlett EL, Smith PH. Effects of paired-pulse and repetitive stimulation on neurons in the rat medial geniculate body. *Neuroscience* 113: 957–974, 2002.

Bazhenov M, Timofeev I, Steriade M, Sejnowski TJ. Model of thalamocortical slow-wave sleep oscillations and transitions to activated states. *J Neurosci* 22: 8691–8704, 2002.

Bereshpolova Y, Stoelzel CR, Zhuang J, Amitai Y, Alonso JM, Swadlow HA. Getting drowsy? Alert/nonalert transitions and visual thalamocortical network dynamics. *J Neurosci* 31: 17480–17487, 2011.

Bickford ME, Günlük AE, van Horn SC, Sherman SM. GABAergic projection from the basal forebrain to the visual sector of the thalamic reticular nucleus in the cat. *J Comp Neurol* 348: 481–510, 1994.

Boudreau CE, Ferster D. Short-term depression in thalamocortical synapses of cat primary visual cortex. *J Neurosci* 25: 7179–7190, 2005.

Bruno RM, Sakmann B. Cortex is driven by weak but synchronously active thalamocortical synapses. *Science* 312: 1622–1627, 2006.

Cellucci C, Albano AM, Rapp P. Statistical validation of mutual information calculations: comparison of alternative numerical algorithms. *Phys Rev E* 71: 066208, 2005.

Chance FS, Nelson SB, Abbott LF. Synaptic depression and the temporal response characteristics of V1 cells. *J Neurosci* 18: 4785–4799, 1998.

Chen C, Regehr WG. Presynaptic modulation of the retinogeniculate synapse. *J Neurosci* 23: 3130–3135, 2003.

Ching S, Cimenser A, Purdon PL, Brown EN, Kopell NJ. Thalamocortical model for a propofol-induced α-rhythm associated with loss of consciousness. *Proc Natl Acad Sci USA* 107: 22665–22670, 2010.

Chung S, Li X, Nelson SB. Short-term depression at thalamocortical synapses contributes to rapid adaptation of cortical sensory responses in vivo. *Neuron* 34: 437–446, 2002.

Crabtree JW, Isaac JT. New intrathalamic pathways allowing modality-related and cross-modality switching in the dorsal thalamus. *J Neurosci* 22: 8754–8761, 2002.

Crandall SR, Cruikshank SJ, Connors BW. A corticothalamic switch: controlling the thalamus with dynamic synapses. *Neuron* 86: 768–782, 2015.

Crandall SR, Govindaiah G, Cox CL. Low-threshold Ca^{2+} current amplifies distal dendritic signaling in thalamic reticular neurons. *J Neurosci* 30: 15419–15429, 2010.

Crick F. Function of the thalamic reticular complex: the searchlight hypothesis. *Proc Natl Acad Sci USA* 81: 4586–4590, 1984.

Cruikshank SJ, Lewis TJ, Connors BW. Synaptic basis for intense thalamocortical activation of feedforward inhibitory cells in neocortex. *Nat Neurosci* 10: 462–468, 2007.

Cucchiaro JB, Bickford ME, Sherman SM. A GABAergic projection from the pretectum to the dorsal lateral geniculate nucleus in the cat. *Neuroscience* 41: 213–226, 1991.

Darbellay GA, Vajda I. Estimation of the information by an adaptive partitioning of the observation space. *IEEE Trans Inf Theory* 45: 1315–1321, 1999.

Davidson S, Zhang X, Yoon CH, Khasabov SG, Simone DA, Giesler GJ. The itch-producing agents histamine and cowhage activate separate populations of primate spinothalamic tract neurons. *J Neurosci* 27: 10007–10014, 2007.

Deleuze C, David F, Béhuret S, Sadoc G, Shin HS, Uebele VN, Renger JJ, Lambert RC, Leresche N, Bal T. T-type calcium channels consolidate tonic action potential output of thalamic neurons to neocortex. *J Neurosci* 32: 12228–12236, 2012.

Denning KS, Reinagel P. Visual control of burst priming in the anesthetized lateral geniculate nucleus. *J Neurosci* 25: 3531–3538, 2005.

Deschênes M, Madariaga-Domich A, Steriade M. Dendrodendritic synapses in the cat reticularis thalami nucleus: a structural basis for thalamic spindle synchronization. *Brain Res* 334: 165–168, 1985.

Destexhe A, Bal T, McCormick DA, Sejnowski TJ. Ionic mechanisms underlying synchronized oscillations and propagating waves in a model of ferret thalamic slices. *J Neurophysiol* 76: 2049–2070, 1996.

Destexhe A, Contreras D, Sejnowski TJ, Steriade M. A model of spindle rhythmicity in the isolated thalamic reticular nucleus. *J Neurophysiol* 72: 803–818, 1994.

Destexhe A, Contreras D, Steriade M. Mechanisms underlying the synchronizing action of corticothalamic feedback through inhibition of thalamic relay cells. *J Neurophysiol* 79: 999–1016, 1998.

Destexhe A, McCormick DA, Sejnowski TJ. A model for 8–10 Hz spindling in interconnected thalamic relay and reticularis neurons. *Biophys J* 65: 2473–2477, 1993.

Destexhe A, McCormick DA, Sejnowski TJ. Thalamic and thalamocortical mechanisms underlying 3 Hz spike-and-wave discharges. *Prog Brain Res* 121: 289–307, 1999.

Fanselow EE, Sameshima K, Baccala LA, Nicolelis MA. Thalamic bursting in rats during different awake behavioral states. *Proc Natl Acad Sci USA* 98: 15330–15335, 2001.

Funke K, Eysel UT, FitzGibbon T. Retinogeniculate transmission by NMDA and non-NMDA receptors in the cat. *Brain Res* 547: 229–238, 1991.

Gentet LJ, Ulrich D. Strong, reliable and precise synaptic connections between thalamic relay cells and neurones of the nucleus reticularis in juvenile rats. *J Physiol* 546: 801–811, 2003.

Gentet L, Ulrich D. Electrophysiological characterization of synaptic connections between layer VI cortical cells and neurons of the nucleus reticularis thalami in juvenile rats. *Eur J Neurosci* 19: 625–633, 2004.

Gil Z, Amitai Y. Adult thalamocortical transmission involves both NMDA and non-NMDA receptors. *J Neurophysiol* 76: 2547–2554, 1996.

Gil Z, Connors BW, Amitai Y. Differential regulation of neocortical synapses by neuromodulators and activity. *Neuron* 19: 679–686, 1997.

Gil Z, Connors BW, Amitai Y. Efficacy of thalamocortical and intracortical synaptic connections: quanta, innervation, and reliability. *Neuron* 23: 385–397, 1999.

Goense J, Ratnam R, Nelson ME. Burst firing improves the detection of weak signals in spike trains. *Neurocomputing* 52: 103–108, 2003.

Grillner S, Buchanan JT, Lansner A. Simulation of the segmental burst generating network for locomotion in lamprey. *Neurosci Lett* 89: 31–35, 1988.

Guido W, Lu SM, Vaughan J, Godwin DW, Sherman SM. Receiver operating characteristic (ROC) analysis of neurons in the cat's lateral geniculate nucleus during tonic and burst response mode. *Vis Neurosci* 12: 723–741, 1995.

Guido W, Weyand T. Burst responses in thalamic relay cells of the awake behaving cat. *J Neurophysiol* 74: 1782–1786, 1995.

Guillery RW, Feig SL, Lozsádi DA. Paying attention to the thalamic reticular nucleus. *Trends Neurosci* 21: 28–32, 1998.

Halassa MM, Chen Z, Wimmer RD, Brunetti PM, Zhao S, Zikopoulos B, Wang F, Brown EN, Wilson MA. State-dependent architecture of thalamic reticular subnetworks. *Cell* 158: 808–821, 2014.

Halassa MM, Siegle JH, Ritt JT, Ting JT, Feng G, Moore CI. Selective optical drive of thalamic reticular nucleus generates thalamic bursts and cortical spindles. *Nat Neurosci* 14: 1118–1120, 2011.

Hänggi P. Stochastic resonance in biology. How noise can enhance detection of weak signals and help improve biological information processing. *Chem Phys Chem* 3: 285–290, 2002.

Hirata A, Castro-Alamancos MA. Relief of synaptic depression produces long-term enhancement in thalamocortical networks. *J Neurophysiol* 95: 2479–2491, 2006.

Hirsch JC, Fourment A, Marc ME. Sleep-related variations of membrane potential in the lateral geniculate body relay neurons of the cat. *Brain Res* 259: 308–312, 1983.

Hubel DH. Single unit activity in lateral geniculate body and optic tract of unrestrained cats. *J Physiol* 150: 91–104, 1960.

Huguenard J, Prince D. A novel T-type current underlies prolonged Ca^{2+}-dependent burst firing in GABAergic neurons of rat thalamic reticular nucleus. *J Neurosci* 12: 3804–3817, 1992.

Huguenard JR. Neuronal circuitry of thalamocortical epilepsy and mechanisms of antiabsence drug action. *Adv Neurol* 79: 991–999, 1998.

Jahnsen H, Llinas R. Electrophysiological properties of guinea-pig thalamic neurones: an in vitro study. *J Physiol* 349: 205–226, 1984.

Jeanmonod D, Magnin M, Morel A. Low-threshold calcium spike bursts in the human thalamus. Common physiopathology for sensory, motor and limbic positive symptoms. *Brain* 119: 363–375, 1996.

Jones EG. *The Thalamus*. Cambridge, UK: Cambridge Univ. Press, 2007.

Kao CQ, Coulter DA. Physiology and pharmacology of corticothalamic stimulation-evoked responses in rat somatosensory thalamic neurons in vitro. *J Neurophysiol* 77: 2661–2676, 1997.

Kimura A. Diverse subthreshold cross-modal sensory interactions in the thalamic reticular nucleus: implications for new pathways of cross-modal attentional gating function. *Eur J Neurosci* 39: 1405–1418, 2014.

Kimura A, Imbe H, Donishi T, Tamai Y. Axonal projections of single auditory neurons in the thalamic reticular nucleus: implications for tonotopy-related gating function and cross-modal modulation. *Eur J Neurosci* 26: 3524–3535, 2007.

Krahe R, Gabbiani F. Burst firing in sensory systems. *Nat Rev Neurosci* 5: 13–23, 2004.

Landisman CE, Long MA, Beierlein M, Deans MR, Paul DL, Connors BW. Electrical synapses in the thalamic reticular nucleus. *J Neurosci* 22: 1002–1009, 2002.

Laurent A, Goaillard JM, Cases O, Lebrand C, Gaspar P, Ropert N. Activity-dependent presynaptic effect of serotonin 1B receptors on the somatosensory thalamocortical transmission in neonatal mice. *J Neurosci* 22: 886–900, 2002.

Lesica NA, Stanley GB. Encoding of natural scene movies by tonic and burst spikes in the lateral geniculate nucleus. *J Neurosci* 24: 10731–10740, 2004.

Lesica NA, Weng C, Jin J, Yeh CI, Alonso JM, Stanley GB. Dynamic encoding of natural luminance sequences by LGN Bursts. *PLoS Biol* 4: e209, 2006.

Lisman JE. Bursts as a unit of neural information: making unreliable synapses reliable. *Trends Neurosci* 20: 38–43, 1997.

Liu RC, Tzonev S, Rebrik S, Miller KD. Variability and information in a neural code of the cat lateral geniculate nucleus. *J Neurophysiol* 86: 2789–2806, 2001.

Liu XB, Jones EG. Predominance of corticothalamic synaptic inputs to thalamic reticular nucleus neurons in the rat. *J Comp Neurol* 414: 67–79, 1999.

Livingstone M, Hubel DH. Effects of sleep and arousal on the processing of visual information in the cat. *Nature* 291: 554–561, 1981.

Llano DA, Slater BJ, Lesicko AM, Stebbings KA. An auditory colliculothalamocortical brain slice preparation in mouse. *J Neurophysiol* 111: 197–207, 2014.

Llinás RR, Paré D. Of dreaming and wakefulness. *Neuroscience* 44: 521–535, 1991.

Lu SM, Guido W, Sherman SM. Effects of membrane voltage on receptive field properties of lateral geniculate neurons in the cat: contributions of the low-threshold Ca^{2+} conductance. *J Neurophysiol* 68: 2185, 1992.

Lüthi A, McCormick DA. H-current: properties of a neuronal and network pacemaker. *Neuron* 21: 9–12, 1998.

Marek T, Tichavsky P. On the estimation of mutual information. In: *Proceedings of ROBUST*. Prague: JCMF, 2008.

Marlinski V, Beloozerova IN. Burst firing of neurons in the thalamic reticular nucleus during locomotion. *J Neurophysiol* 112: 181–192, 2014.
McAlonan K, Cavanaugh J, Wurtz RH. Attentional modulation of thalamic reticular neurons. *J Neurosci* 26: 4444–4450, 2006.
McAlonan K, Cavanaugh J, Wurtz RH. Guarding the gateway to cortex with attention in visual thalamus. *Nature* 456: 391–394, 2008.
McCormick DA, Contreras D. On the cellular and network bases of epileptic seizures. *Annu Rev Physiol* 63: 815–846, 2001.
Miller LM, Escabi MA, Read HL, Schreiner CE. Functional convergence of response properties in the auditory thalamocortical system. *Neuron* 32: 151–160, 2001.
Moore JW, Ramon F. On numerical integration of the Hodgkin and Huxley equations for a membrane action potential. *J Theor Biol* 45: 249–273, 1974.
Mukherjee P, Kaplan E. Dynamics of neurons in the cat lateral geniculate nucleus: in vivo electrophysiology and computational modeling. *J Neurophysiol* 74: 1222–1243, 1995.
Nelder JA, Mead R. A simplex method for function minimization. *Comput J* 7: 308–313, 1965.
Ortuño T, Grieve KL, Cao R, Cudeiro J, Rivadulla C. Bursting thalamic responses in awake monkey contribute to visual detection and are modulated by corticofugal feedback. *Front Behav Neurosci* 8: 198, 2014.
Person AL, Perkel DJ. Unitary IPSPs drive precise thalamic spiking in a circuit required for learning. *Neuron* 46: 129–140, 2005.
Peruzzi D, Bartlett E, Smith PH, Oliver DL. A monosynaptic GABAergic input from the inferior colliculus to the medial geniculate body in rat. *J Neurosci* 17: 3766–3777, 1997.
Pinault D. The thalamic reticular nucleus: structure, function and concept. *Brain Res Rev* 46: 1–31, 2004.
Pinault D, Deschênes M. Anatomical evidence for a mechanism of lateral inhibition in the rat thalamus. *Eur J Neurosci* 10: 3462–3469, 1998.
Pita-Almenar JD, Yu D, Lu HC, Beierlein M. Mechanisms underlying desynchronization of cholinergic-evoked thalamic network activity. *J Neurosci* 34: 14463–14474, 2014.
Pospischil M, Toledo-Rodriguez M, Monier C, Piwkowska Z, Bal T, Frégnac Y, Markram H, Destexhe A. Minimal Hodgkin-Huxley type models for different classes of cortical and thalamic neurons. *Biol Cybern* 99: 427–441, 2008.
Ramcharan EJ, Gnadt JW, Sherman SM. Burst and tonic firing in thalamic cells of unanesthetized, behaving monkeys. *Vis Neurosci* 17: 55–62, 2000.
Ramcharan EJ, Gnadt JW, Sherman SM. Higher-order thalamic relays burst more than first-order relays. *Proc Natl Acad Sci USA* 102: 12236–12241, 2005.
Reichova I, Sherman SM. Somatosensory corticothalamic projections: distinguishing drivers from modulators. *J Neurophysiol* 92: 2185–2197, 2004.
Reig R, Gallego R, Nowak LG, Sanchez-Vives MV. Impact of cortical network activity on short-term synaptic depression. *Cereb Cortex* 16: 688–695, 2006.
Reinagel P, Godwin D, Sherman SM, Koch C. Encoding of visual information by LGN bursts. *J Neurophysiol* 81: 2558–2569, 1999.
Rose JE, Greenwood DD, Goldberg JM, Hind JE. Some discharge characteristics of single neurons in the inferior colliculus of the cat. I. Tonotopical organization, relation of spike-counts to tone intensity, and firing patterns of single elements. *J Neurophysiol* 26: 294–320, 1963.
Sherman SM. Tonic and burst firing: dual modes of thalamocortical relay. *Trends Neurosci* 24: 122–126, 2001.
Sherman SM. Interneurons and triadic circuitry of the thalamus. *Trends Neurosci* 27: 670–675, 2004.
Shosaku A, Sumitomo I. Auditory neurons in the rat thalamic reticular nucleus. *Exp Brain Res* 49: 432–442, 1983.
Sillito AM, Cudeiro J, Jones HE. Always returning: feedback and sensory processing in visual cortex and thalamus. *Trends Neurosci* 29: 307–316, 2006.
Sincich LC, Adams DL, Economides JR, Horton JC. Transmission of spike trains at the retinogeniculate synapse. *J Neurosci* 27: 2683–2692, 2007.
Smith GD, Cox CL, Sherman SM, Rinzel J. Fourier analysis of sinusoidally driven thalamocortical relay neurons and a minimal integrate-and-fire-or-burst model. *J Neurophysiol* 83: 588–610, 2000.
Stacey WC, Durand DM. Stochastic resonance improves signal detection in hippocampal CA1 neurons. *J Neurophysiol* 83: 1394–1402, 2000.
Steriade M, McCormick D, Sejnowski T. Thalamocortical oscillations in the sleeping and aroused brain. *Science* 262: 679–685, 1993a.
Steriade M, Nunez A, Amzica F. Intracellular analysis of relations between the slow (<1 Hz) neocortical oscillation and other sleep rhythms of the electroencephalogram. *J Neurosci* 13: 3266–3283, 1993b.
Stratford KJ, Tarczy-Hornoch K, Martin KAC, Bannister NJ, Jack JJ. Excitatory synaptic inputs to spiny stellate cells in cat visual cortex. *Nature* 382: 258–261, 1996.
Suga N, Ma X. Multiparametric corticofugal modulation and plasticity in the auditory system. *Nat Rev Neurosci* 4: 783–794, 2003.
Sun QQ, Huguenard JR, Prince DA. Barrel cortex microcircuits: thalamocortical feedforward inhibition in spiny stellate cells is mediated by a small number of fast-spiking interneurons. *J Neurosci* 26: 1219–1230, 2006.
Sun YG, Pita-Almenar JD, Wu CS, Renger JJ, Uebele VN, Lu HC, Beierlein M. Biphasic cholinergic synaptic transmission controls action potential activity in thalamic reticular nucleus neurons. *J Neurosci* 33: 2048–2059, 2013.
Swadlow H, Gusev A. The impact of "bursting" thalamic impulses at a neocortical synapse. *Nat Neurosci* 4: 402–408, 2001.
Tsodyks MV, Markram H. The neural code between neocortical pyramidal neurons depends on neurotransmitter release probability. *Proc Natl Acad Sci USA* 94: 719–723, 1997.
Turner JP, Salt TE. Characterization of sensory and corticothalamic excitatory inputs to rat thalamocortical neurones in vitro. *J Physiol* 510: 829–843, 1998.
Venkataraman Y, Bartlett EL. Postnatal development of synaptic properties of the GABAergic projection from the inferior colliculus to the auditory thalamus. *J Neurophysiol* 109: 2866–2882, 2013.
von Krosigk M, Bal T, McCormick D. Cellular mechanisms of a synchronized oscillation in the thalamus. *Science* 261: 361–364, 1993.
Wanaverbecq N, Bodor ÁL, Bokor H, Slézia A, Lüthi A, Acsády L. Contrasting the functional properties of GABAergic axon terminals with single and multiple synapses in the thalamus. *J Neurosci* 28: 11848–11861, 2008.
Wang X, Wei Y, Vaingankar V, Wang Q, Koepsell K, Sommer FT, Hirsch JA. Feedforward excitation and inhibition evoke dual modes of firing in the cat's visual thalamus during naturalistic viewing. *Neuron* 55: 465–478, 2007.
Wang XJ. Multiple dynamical modes of thalamic relay neurons: rhythmic bursting and intermittent phase-locking. *Neuroscience* 59: 21–31, 1994.
Watson BO, MacLean JN, Yuste R. UP states protect ongoing cortical activity from thalamic inputs. *PLoS One* 3: e3971, 2008.
Wehr M, Zador AM. Synaptic mechanisms of forward suppression in rat auditory cortex. *Neuron* 47: 437–445, 2005.
Willis A, Llano D. Enhanced thalamocortical activity secondary to thalamic reticular nucleus activation: a computational model (Abstract). *Neuroscience Meeting Planner* 2012: Abstract 368.16, 2012.
Winer JA, Saint Marie RL, Larue DT, Oliver DL. GABAergic feedforward projections from the inferior colliculus to the medial geniculate body. *Proc Natl Acad Sci USA* 93: 8005–8010, 1996.
Wolfart J, Debay D, Le Masson G, Destexhe A, Bal T. Synaptic background activity controls spike transfer from thalamus to cortex. *Nat Neurosci* 8: 1760–1767, 2005.
Yamada WM, Koch C, Adams PR. Multiple channels and calcium dynamics. In: *Methods in Neuronal Modeling*. Cambridge, MA: MIT Press, 1989, p. 97–133.
Yu XJ, Xu XX, Chen X, He S, He J. Slow recovery from excitation of thalamic reticular nucleus neurons. *J Neurophysiol* 101: 980–987, 2009.
Zikopoulos B, Barbas H. Prefrontal projections to the thalamic reticular nucleus form a unique circuit for attentional mechanisms. *J Neurosci* 26: 7348–7361, 2006.
Zikopoulos B, Barbas H. Pathways for emotions and attention converge on the thalamic reticular nucleus in primates. *J Neurosci* 32: 5338–5350, 2012.